Toward efficient and selective thorium recovery using stable ion-imprinting sorbent – application to processed acidic ore leachate as a case study

Mengjie Zhao, Amr Fouda, Khalid A.M. Salih, Guibal Eric, Yuezhou Wei, Shunyan Ning, Mohammed Hamza, Saly El Dakkony

Chemical Engineering Journal 496 (2024) 154045

Contents lists available at ScienceDirect

Chemical Engineering Journal

journal homepage: www.elsevier.com/locate/cej

Toward efficient and selective thorium recovery using stable ion-imprinting sorbent – application to processed acidic ore leachate as a case study

Mengjie Zhao [a,1], Amr Fouda [a,b,1], Khalid A.M. Salih [c,1], Eric Guibal [d,*], Yuezhou Wei [a,e], Shunyan Ning [a], Mohammed F. Hamza [a,*], Saly R. El Dakkony [f]

[a] School of Nuclear Science and Technology, University of South China, Heng Yang 421001, China
[b] Botany and Microbiology Department, Faculty of Science, Al-Azhar University, Nasr City, Cairo 11884, Egypt
[c] School of Metallurgy and Environment. Central South University, Changsha 410083, China
[d] Polymers Composites and Hybrids (PCH), IMT Mines Ales, Alès, France
[e] School of Nuclear Science and Engineering, Shanghai Jiao Tong University, Shanghai, China
[f] Egyptian Mineral Resources Authority, Cairo, Egypt

ARTICLE INFO

Keywords:
Thorium sorption
Ion-imprinting
Vinylphosphonic acid/acrylamides-based resin
Selectivity enhancement
Stability at recycling
Thorium recovery from complex solutions

ABSTRACT

The recovery of thorium from aqueous industrial effluents is a challenge not only for environmental purpose but also for the valorization of secondary resources. The complexity of these effluents not only require designing highly efficient stable sorbent with highly reactive functional groups but also with good selectivity. Phosphonic groups are efficient for the binding of thorium. Successive grafting of phosphonic groups through one-pot reaction of vinylphosphonic acid with acrylamide-based reagents (as monomer and crosslinker) for polymerizing an efficient sorbent (HVP/NIP) toward Th(IV) recovery in slightly acidic solution. On the other hand, the selectivity objective was reached by adopting an ion-imprinting strategy (HVP/IP). While the templating weakly improves sorption capacity (at 1.46 mmol g^{-1} at pH close to 3), the most significant benefits concern the uptake kinetics (slightly enhanced; equilibrium being reached in 20–25 min) and more significantly the separation properties of HVP/IP, against base metals and uranium (to a certain extent). The selectivity coefficient (i.e., $SC_{Th/metal}$) increases twice (against U and Ca) and up to 16-folds against Al, at pH_0 3. Fourier-transform infrared and XPS spectroscopy confirm the structural differences for both sorbents (arrangement of reactive groups) and the interactions modes involved in thorium binding mechanisms. The remarkable sorption properties of HVP/IP are also illustrated by the good stability of the sorbent at recycling (loss in sorption less than 2% at the 10^{th} cycle): complete desorption is achieved using 0.3 M HNO_3 solution. The ion-imprinted sorbent is successfully applied to the recovery of valuable metals (thorium, uranium, and gallium) from acidic ore leachate at different pH values. The materials are fully characterized using different analytical tools; i.e., FTIR, TGA, XPS, BET, titration, and elemental analysis.

1. Introduction

Thorium is part of the radionuclides that require special attention in mining exploitation and management of secondary pollution (in the surroundings of mining areas) [1,2]. Frequently associated with uranium and rare earth elements (REEs) [2,3], its separation from base metals (and other valuable metals) is of critical importance [4,5]. Recently, a regain of interest has been given to thorium due to promising perspectives for designing new nuclear power plants [6–8].

The recovery of thorium from mining ores usually requires acidic leaching [9–12]. These acidic leachates may contain huge concentrations of base metals apart thorium, uranium, and rare earth elements. Based on concentration levels, processes such as precipitation [4,13] or solvent extraction [4,9,13–15] are generally applied for the recovery of these valuable metals. In the case of dilute effluents (produced from low grade ores or as residues of precipitation and solvent extraction processes), sorption techniques may be used for the removal of thorium (and associated metals). The last decades have shown the possibility to use biosorbents [16–18], mineral sorbents (raw or functionalized) [19–23], composites [24], ion exchange and chelating resins [25–29],

* Corresponding authors.
E-mail addresses: eric.guibal@mines-ales.fr (E. Guibal), m_fouda21@usc.edu.cn (M.F. Hamza).
[1] Authors with equal contribution.

https://doi.org/10.1016/j.cej.2024.154045
Received 29 March 2024; Received in revised form 12 July 2024; Accepted 15 July 2024
Available online 16 July 2024

for the treatment of thorium-containing effluents (nuclear wastes, leachates, and acid mine drainage). The design of a new sorbent may be oriented by analogy with efficient extractants (applied in solvent extraction) and by the proper coordination properties of specific functional groups for thorium complexation [30–32]. A wide diversity of reactive groups may be mobilized for the binding of thorium. Table S1 (see Supplementary Information) lists a series of sorbents bearing different functional groups with their maximum sorption capacity for Th (IV). A number of amine- and amide-based sorbents were investigated; however, the most promising involved organophosphorus compounds [33,34], amidoxime [35], or S-bearing groups [36].

In the current work, the strategy consisted in synthesizing a bifunctional sorbent bearing both amide groups and phosphonic acid moieties, which are efficient for Th(IV) sorption (based on literature survey). The new sorbent (herein designed HVP) was obtained by free radical polymerization (assisted by MBA crosslinking) involving three precursors: N-(hydroxymethyl) acrylamide, *N,N'*-methylenebisacrylamide and vinyl phosphonic acid. An important challenge concerns the selective properties of the sorbent and its capacity to separate thorium from other metal ions usually present in acid mine drainage and leachates (including the recovery and separation of uranium and REEs from base metals). The first step for improving selective properties consists of the appropriate selection of functional groups (based on Pearson' principles, hard and soft acid base theory [37]). Thorium (as well as uranium) is classified among hard Lewis acid (according HSAB); consequently, Th (IV) coordinates preferentially with hard Lewis bases such as those bearing oxygen and nitrogen donor atoms. It is thus possible anticipating that amide and phosphonic-based functional groups preferentially bind Th (and U) against soft Lewis acid (such as Cd, Ag, Cs, etc.) and borderline metal ions (divalent cations, for example: Co, Ni, Cu, Zn, Pb, etc.). However, it is also possible enhancing the selectivity through ion-imprinting methods [38–41]. This method has been recently applied for designing sorbents for selective thorium recovery [42,43]. The concept is based on the synthesis of the resin in the presence of target metal ion (herein Th(IV)) followed by the leaching of the template metal. This process allows orienting the polymerization of precursors through alternative reactive groups (maintaining free those reactive groups initially bound to the metal), but also to save a physical cavity of geometry favorable to the Th(IV) target. To evaluate the beneficial effect of ion-imprinting on Th(IV) removal (and separation), the sorption properties are compared for HVP sorbent under non-imprinted (HVP/NIP) and imprinted (HVP/IP) forms. The sorption properties are evaluated through the study of pH effect, uptake kinetics, sorption isotherms (at different temperatures), metal desorption and sorbent recycling. The selective properties are investigated using multi-component synthetic (equimolar) solutions before applying the process to the treatment of an acidic ore leachate. The characteristics of the sorbents and their interactions with thorium are analyzed with a mix of techniques (textural properties by N_2 isotherms of adsorption and desorption, thermogravimetric analysis, Fourier transform infrared spectrometry, X-ray photoelectron spectrometry, elemental analysis, titration for determination of pH_{pzc}).

2. Materials and methods

2.1. Materials

Vinylphosphonic acid (VPA, 97 %), N-(hydroxymethyl) acrylamide (HMAA, 48 % aqueous solution), *N,N'*-methylenebisacrylamide (MBA, 99 %), methyl benzoate (99 %), 2,2'-azobis(2-methylpropionitrile) (AIBN, 98 %), hydrochloric acid (HCl; 37 %), acetone (>99.5 %), and sodium hydroxide (>97.0 %) from Sigma-Aldrich (Merck, KGa; Darmstadt, Germany). Thorium nitrate (hydrated) (>99 %) was supplied by Otto-Chemie, Pvt, Ltd (Popatwadi, Mumbai, India). Uranyl nitrate (hexahydrate) was purchased from SPI Supplies (West Chester, PA, USA). Calcium chloride (>99.1 %), cadmium chloride (99.99 %), and lead chloride (98 %) were obtained from Shanghai Makclin-Biochemical Co., Ltd. (Shanghai, China). Iron (III) chloride (97.0 %), zinc chloride (98.0 %), and aluminum chloride (99.1 %) were purchased from Guangdong-Guanghua, Sci-Tech Co.-Ltd. (Guangdong, China).

2.2. Synthesis and characterization of sorbents

The (ion imprinted polymer) IIP was synthesized by mixing equimolar amounts (60 mmol) of HMAA (i.e., 12.6 g) and VPA (i.e., 6.7 g) in water (50 mL). This mixture is stirred at 323 K for 1 h (up to complete dissolution). Afterwards, 100 mL of 1 g L^{-1} of thorium nitrate solution was added drop wise (in 30 min) under continuous stirring (250 rpm) and the mixture was kept under stirring for further 5 h. A fixed amount (20 mmol, 3.1 g) of MBA (as a crosslinking agent) was added to the mixture and stirred for further 5 h, followed by the addition of 50 mL methyl benzoate solution (as a pore producing solvent). AIBN (0.2 g, initiator) was added to the mixture then the reaction was carried out at 253 K for 7 h. The produced hydrogel was filtered, washed with water and acetone before the next step (metal elution). The obtained precipitate was mixed with 0.5 M HNO_3 solution for removing the template ions before washing several times with water and acetone. The product was then dried at 333 K (the yield was 15.5 g, d.w.). Scheme 1a shows the sequence of synthesis steps. The same procedure was applied for the preparation of HVP/NIP (without templates), as shown in Scheme 1b. The yield reached 13.1 g (d.w.).

Many studies pointed out the interest of acrylamide for the synthesis of functional polymers. Indeed, acrylamide moiety is highly reactive and provides many possibilities for coupling with other monomers. On the other hand, the presence of terminal vinyl groups in poly(vinylphosphonic acid) (PVPA) and N-(hydroxymethyl) acrylamide makes these precursors highly reactive and suitable for simple free radical polymerization [44,45]. The synthesized copolymer contains phosphonic acid (which are considered as proton donor group) that enhance sorption toward metal ions and improved proton conductivity (for further application) [46,47]. On the other hand, the functional crosslinking agent (MBA) increases the flexibility of rigid polymer networks [48]. Birlik et al. [49] prepared chitosan-based ion-imprinted sorbent for selective thorium recovery; they pointed out the interest of the flexibility of the biopolymer for enabling the sorbent to adopt the appropriate configuration for metal binding. The presence of terminal vinyl groups on VPA and acrylamides (both MBA and HMAA) explains the high reactivity of the precursors for free radical polymerization and the easy synthesis of the sorbent. Though methods were developed for preparing ion-imprinted sorbents (such as entrapment technologies, [50] or chemical modification of ligands to bring polymerizable moieties), vinyl-bearing ligands are usually preferred [51]. The flexibility of the polymer (which makes easy the shaping of the polymer for forming appropriate cavity in presence of thorium) is favored by MBA that improves the flexibility of the polymeric structure. The presence of phosphonate groups is also highly favorable to the interaction of with radionuclides such as uranium, thorium, and rare earth elements (for complexation, precipitation, or sorption) [52–57]. The existence of carbonyl and amide groups in the near environment of phosphonate moieties may also contribute to complementary reactivity and modulation of hydrophilic, and acid/base properties [58].

The characterization of the materials is fully described in the Supplementary Information (Text S1): textural, properties, thermogravimetric, scanning electron microscopy, Fourier-Transform InfraRed (FTIR) and X-ray photoelectron (XPS) spectrometry, elemental composition, and titration (pH_{pzc}).

2.3. Study of sorption properties

Sorption experiments were performed in batch systems. A fixed volume of solution (V, L), at given concentration of metal (C_0, mmol L^{-1}) and controlled pH value (using 0.1/1 M HCl and NaOH solutions), was

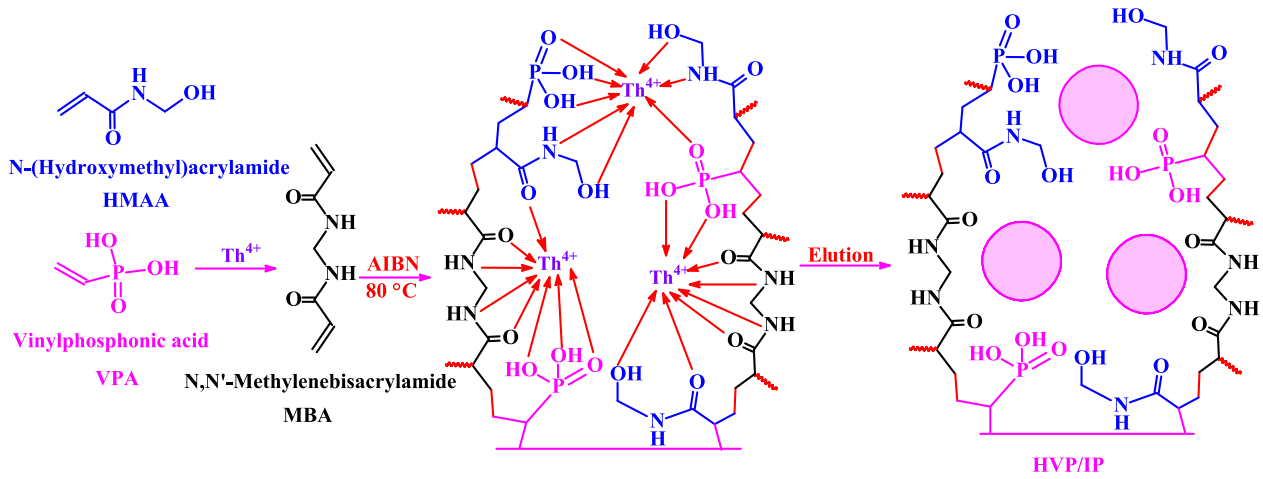

Scheme 1a. Synthesis of HVP/IP.

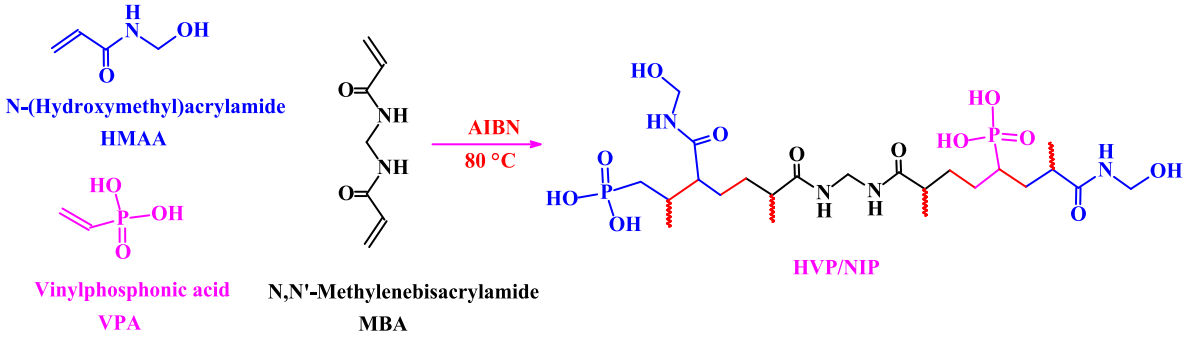

Scheme 1b. Synthesis of HVP/NIP.

mixed with a fixed amount of sorbent (m, g; sorbent dose, SD=m/V, g L^{-1}). Unless specified, the temperature was set at 294 K, and the agitation speed was maintained at 210 rpm. After fixed contact times (for kinetics) or 24/48 h (for equilibrium tests), samples were collected and filtrated (1.2 μm pore size membrane filter) and the residual concentration (C_{eq}, mmol L^{-1}) was determined by ICP-AES (inductively coupled plasma atomic emission spectrometry, ICPS-7510, Shimadzu, Tokyo, Japan). The sorption capacity (q, mmol g^{-1}) was deduced by the mass balance equation: $q = (C_0\text{-}C_{eq}) \times V/m$. Similar procedure was applied for multicomponent solutions (prepared with equimolar concentration (i.e., 1 mmol L^{-1}) of each competitor metal/metalloid ion). The pH was not controlled during sorption experiments, but the equilibrium pH was systematically monitored. The Th-loaded samples collected from kinetic experiments were used for the study of metal desorption and sorbent recycling. The sorbent dose was set to 0.5 g L^{-1} for uptake kinetics, while desorption tests were performed with a sorbent dose of 1.3 g L^{-1}. The volume of the eluent was reduced for increasing sorbent dose and concentrating thorium in the eluate. Sorption tests were duplicated; the experiments showed good reproducibility as shown by error bars (displayed in the figures). Detailed experimental conditions are systematically reported in the caption of the figures.

The equations used for the modeling of uptake kinetics and sorption isotherms are summarized in Tables S2a and S2b, respectively. The parameters of these models were determined by nonlinear regression analysis (using the facilities of Mathematica™ software and proprietary notebooks). The "quality" of the fits was evaluated and compared using both the determination coefficient (i.e., R^2) and the Akaike Information Criterion (i.e., AIC).

2.4. Application to ore leachate

The ore sample can be considered as a "typical rare earth mining" mineral. It is essentially constituted of ferrocolumbite, cassiterite, zircon, tantalite, autunite, thorite and uranothorite, with REEs being found in xenotime, monazite and bastnaesite minerals.

The ore sample was grinded and sieved; the fraction (−50/-70 Mesh; 212–300 μm) was collected and tested for acid leaching. The sample (1 kg) was mixed with 4 L of 7 M HCl acid solution for 3 h at 343 ± 2 K. The leachate (3.39 L) was characterized for metal (and metalloid) contents using ICP-AES (7510 ICP, Shimadzu Instruments, Tokyo, Japan) for U and other metals, while sodium was analyzed by flame atomic absorption spectrophotometry (FAAS AA-7000 spectrophotometer, Shimadzu, Tokyo, Japan).

The pH of the leachate was adjusted to fixed values (in the range 1–5) using 0.1/1 M NH_3 or HCl solutions. Ammonia was used for pH control to prevent the shielding effect that could occur with NaOH (or KOH). Sorption tests were performed in batch systems using the method described above. With pH increase the precipitation of some metal ions (Fe(III) and Al(III)) was observed, involving also the co-precipitation of other metal ions. For the calculation of sorption performances (sorption yield, and sorption capacity), the effective concentration of the metals (meaning after partial precipitation) was systematically used.

3. Results and discussion

3.1. Characterization of sorbents

3.1.1. Physical properties

The morphology and the size of sorbent particles can be visualized in

Figure S1 (which shows scanning electron microscopy photos). The particles are rounded with irregular external texture. A large dispersion in size is observed in the size distribution with large agglomerates, (which may reach up to 115 μm); however, the most representative fractions (smallest particles) give average dimensions around 4.3 ± 2.9 μm for HVP/IP and 5.0 ± 3.1 μm for HVP/NIP.

For HVP/NIP, the profile of N_2 adsorption and desorption isotherms corresponds to Type IV(a) shape. This type of isotherm usually describes mesoporous sorbents, where gas adsorption is controlled first by the interactions of sorbent and sorbate, but also by the proper interactions between condensed molecules. The beginning of the linear section (the so-called Point B) is poorly detectable; meaning that the formation of the monolayer at the surface of the sorbent is hardly detectable (associated with the weak interaction of N_2 with the sorbent surface and the overlapped coverage of the monolayer with the formation of multilayer sorption). The hysteresis is well-marked; indicating that the pore size exceeds ≈ 4 nm [59]. The ion-imprinting process significantly changes the profile of the isotherms in the second part of the curves (i.e., at $p/p_0 > 0.85$): the short saturation plateau observed for HVP/NIP disappears with the ion-imprinting; in addition, the hysteresis loop is strongly weakened. This is first evidence that the procedure changes the physical arrangement of the polymer. The specific surface area is hardly changed (from 64.4 to 66.0 $m^2\ g^{-1}$). The pore volume, measured on the adsorption branch, slightly increases (from 0.71 to 0.79 $cm^3\ g^{-1}$); however, the ion-imprinting introduces a strong divergence when considering the desorption branch: the pore volume stable at 0.71 $cm^3\ g^{-1}$ for HVP/NIP dropped down to 0.33 $cm^3\ g^{-1}$. This trend is also observed for the evaluation of pore size, which is higher for ion-imprinted sorbent (514 Å *vs.* 464 Å) for adsorption branch, while for desorption branch the pore size is larger for non-imprinted sorbent (274 Å *vs.* 223 Å). The ion-imprinting increases the size gap between adsorption and desorption branches. Liang et al. [60] also reported a slight improvement in the textural properties of a Th-imprinted sorbent.

3.1.2. Chemical properties

3.1.2.1. Thermogravimetric analysis (TGA). Fig. S3a compares the thermogravimetric analysis (weight loss) of the reference material HVP/NIP with the degradation profiles of the ion-imprinted polymer (i.e., HVP/IP) and the Th-imprinted polymer (prior to the removal of the template; herein noted HVP/IP+Th). First, the general pattern of the profiles is roughly similar for HVP/NIP and HVP/IP; however, the ion-imprinting shifts the curve toward both higher thermal stability (lower weight loss) and higher temperatures (the transitions occur at higher temperature, as shown in the table associated with Figure S3). More detailed discussion of TGA profiles is presented in Text S2 (in Supplementary Information).

3.1.2.2. FTIR spectrometry. The comparison of the FTIR spectra for ion-imprinted and reference (non-imprinted) materials (Fig. S4a) shows substantial differences. The functional groups present on HVP materials can be easily identified. In HVP/NIP spectrum, 3 bands are observed at 3387, 3329, and 3150 cm^{-1}, which correspond to $\nu_{asymN\text{-}H}$, $\nu_{symN\text{-}H}$ (both being superposed near 3300 cm^{-1} with contribution of $\nu_{O\text{-}H\cdot\cdot O}$ bonds), and ν^{+}_{NH4}.vibrations [61]. In the case of HVP/IP, the well-resolved bands are replaced with a broad poorly-resolved band. This is a first indication that the templating effect plays not only with the physical arrangement of the polymer (cavity formation) but also with the chemical structure (different interactions between the precursors). In the case of HVP/NIP in the presence of thorium (HVP/NIP(+Th)), the three bands are replaced with a broad band centered around 3424 cm^{-1} (superposition of stretching bands of N–H and O–H bonds, including those of phosphonic groups). The band at 2895 cm^{-1} (assigned to $\nu_{C\text{-}H,\ aliph}$) in HVP/NIP and HVP(+Th) disappears in HVP/IP, being masked by a broad poorly-resolved area. Two other (less-intense) bands are observed at 2953 and 2806 cm^{-1} that correspond to other $\nu_{C\text{-}H}$ vibrations (i.e., C-H_{asym} and C-H_{sym}). In the region 1670–1620 cm^{-1}, a series of bonds can be detected corresponding to −C-N, −C=O (Amide I), and −N–H. In the ion-imprinted polymer, the width of the band is reduced (compared with non-imprinted material): hence, the broad band with an extremum at 1639 cm^{-1} is replaced with a narrower band at 1665 cm^{-1}; apparently, the environment of −N–H and Amide I band is differently affected when the synthesis is operated in presence or absence of thorium. In this region, the spectrum of HVP/NIP(+Th) shows three bands at 1665, 1631, and 1570 cm^{-1}. A broad band with an extremum at 1400 cm^{-1} is observed on HVP/NIP spectrum, the band becomes narrow for HVP/IP material (with an extremum shifted to 1410 cm^{-1}); this band is associated with $\delta_{CH2aliph}$ vibrations (in different environments). The band is found at 1396 cm^{-1} in HVP/NIP(+Th), with a marked additional band at 1348 cm^{-1}. Phosphonic groups are reported at 1273 cm^{-1} ($\nu_{P=O}$), 1107 and 1013 cm^{-1} ($\nu_{P\text{-}O}$) for HVP/NIP [62]; the bands are shifted to 1276, 1090, and 1016 cm^{-1} respectively in the case of HVP/IP. In the case of HVP/NIP(+Th), these bands are identified at 1261, 1096, and 1028 cm^{-1}, respectively. Another typical band is observed at 752 cm^{-1} (representative of $\delta_{O\text{-}H}$ vibration), after ion-imprinting the band moves to 782 cm^{-1} (787 cm^{-1} for HVP/NIP(+Th)). These numerous and significant differences probably mean that synthesis procedure is affected in terms of chemical structure by the presence of thorium. The imprinted template affects not only the geometry of monomers, but also induces restrictions for some groups to participate in cross-linkages (especially for the electron dentate groups; i.e., NH_2) because they are already engaged in the binding of the template. On the other hand, in non-ion-imprinted materials all groups are free for reacting (without selectivity). This causes significant differences in the characterization of chemical groups (intensity and wavelength).

Fig. 1 compares the FTIR spectra of the two sorbents under different conditions (meaning pristine material, after being conditioned at pH 3, after Th(IV) sorption at pH 3, and after 10 cycles of sorption and desorption). In Fig. 1a for HVP/NIP, the protonation of the sorbent and the sorption of Th(IV) significantly change the spectrum in the region 3600–3000 cm^{-1}: the well resolved bands (representative of $\nu_{N\text{-}H}$ and $\nu_{O\text{-}H}$ vibrations) are replaced by a broad band centered at 3424 cm^{-1}. The Amide I band is shifted from 1640 cm^{-1} to 1680 cm^{-1} (maintaining a shoulder around 1660 cm^{-1}); on the opposite hand, Th(IV) sorption involves the appearance of a band at 1701 cm^{-1} (while the intensity of the 1640–1680 cm^{-1} contribution is strongly reduced). The band at 1400 cm^{-1} in pristine sorbent becomes narrow after pH control at 3, and almost disappears after Th(IV) binding. The bands that represent phosphonate groups are also affected by pH control and metal sorption: the bands are significantly shifted from 1273, 1107, and 1013 cm^{-1} to 1261, 1097, and 1032 cm^{-1} (1269, 1103, and 1016 cm^{-1} for protonated sorbent), respectively. The differences observed before and after Th(IV) sorption may be imputed to complementary effects of protonation at pH 3 and direct interaction of phosphonate with Th(IV). The $\delta_{O\text{-}H}$ vibration at 752 cm^{-1} (associated with a shoulder at ≈780 cm^{-1}) is replaced with single narrow peak at 802 cm^{-1} for both protonated and metal-bound sorbents. Independently of the effect of protonation, the most significant changes in FTIR spectra show that Th(IV) binds preferentially to amide and phosphonate groups (though the changes observed for $\nu_{N\text{-}H}$ in 3600–3000 cm^{-1} region tend to indicate that the environment of N–H groups is also affected by thorium binding).

In the case of HVP/IP, substantial changes are also observed in the region of $\nu_{N\text{-}H}$ and $\nu_{O\text{-}H}$. The band at 1665 cm^{-1} is hardly influenced by metal sorption (at 1660 cm^{-1}); Amide I band is less changed than in the case of non-imprinted sorbent. The 1410 cm^{-1} band (i.e., $\delta_{CH2aliph}$ vibrations) is slightly shifted (from 1410 to 1416 and 1429 cm^{-1}). Significant changes can be reported in the environment of phosphonate associated bonds (i.e., $\nu_{P=O}$, $\nu_{P\text{-}O}$) with variations in both relative intensity and wavelengths. The $\delta_{O\text{-}H}$ vibration is also influenced by Th(IV) binding: the band at 781 cm^{-1} is shifted to 800 cm^{-1} after protonation, while after Th(IV) uptake, this band shifts back to 779 cm^{-1} (contrary to

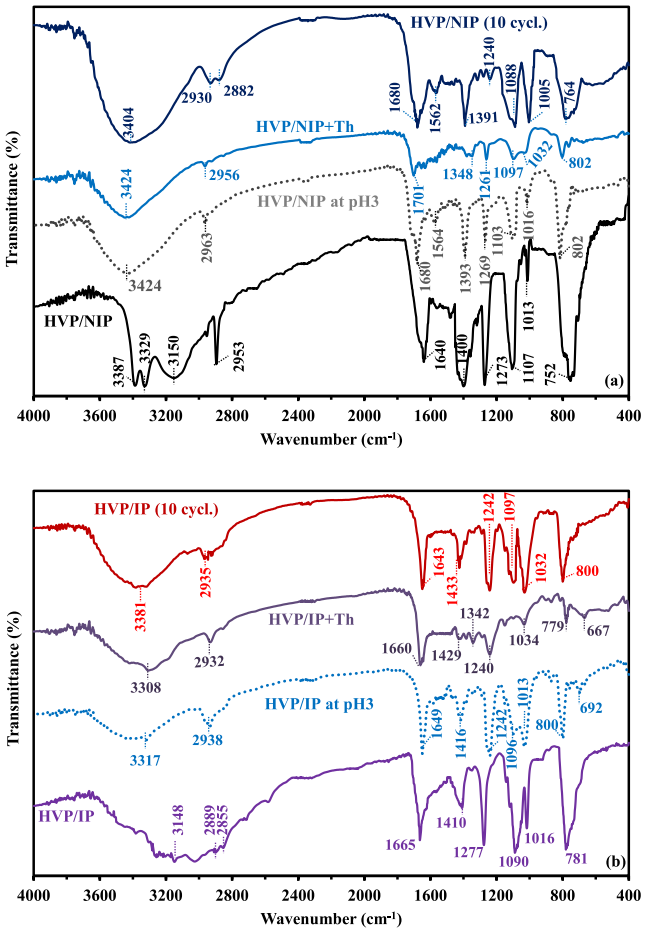

Fig. 1. FTIR spectra of HVP/NIP (a) and HVP/IP (b) as produced, after conditioning at pH 3, after Th(IV) sorption and after 10 cycles of sorption and desorption.

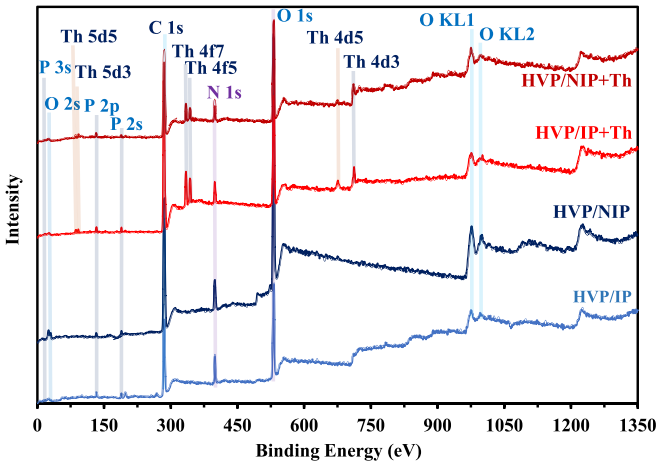

Fig. 2. XPS survey curve for HVP/NIP and HVP/IP sorbents before and after Th (IV) sorption.

HVP/NIP). For both protonated and metal-bound materials, the shoulders at lower wavelengths almost disappear (giving narrower bands).

Based on the modifications of FTIR spectra, the sorption of Th(IV) involves interactions with phosphonate groups, amine/amide groups for both HVP/NIP and HVP/IP. The $\delta_{O\text{-}H}$ vibration is affected by Th(IV) binding differently for the two sorbents: for both of them the shoulders associated with main band disappear, but the wavelength of the main band is not shifted for HVP/IP contrary to HVP/NIP (where the shift is similar to the displacement associated with protonation effect). Fig. S4b discussed in Supplementary information shows the change in FTIR spectrum associated with thorium binding during the synthesis of the templated material.

Fig. 1 also shows the spectra of the sorbents after 10 cycles of sorption and desorption. The comparison of spectra shows that minimal changes are observed on HVP/IP, while the spectrum is more affected by recycling for HVP/NIP. Text S3 (in SI) provides more details on these changes. Apparently, the ion-imprinting contributes to increase the chemical stability of the sorbent when the sorbent is recycled. The polymerization in presence of the template ion orientates the "building" of the sorbent on a way that apparently reinforces its stability.

3.1.2.3. XPS analysis. The organic architecture (HMAA and MBA precursors) is confirmed in the survey XPS spectra (Fig. 2) with the C 1s (at binding energy, BE: 284–285 eV), O 1s (at 498–500 eV), and N1 s (at 399 eV) signals; the effective incorporation of VPA is demonstrated by the appearance of the P 2p signal (at 132–133 eV), completed by the P 2s signal (at 189 eV). On the other hand, the sorption of Th(IV) is highlighted by the appearance of a series of main bands corresponding to the signals Th $4f_{7/2}$ (at 334 eV), Th $4f_{5/2}$ (at 343 eV), Th $4d_{5/2}$ (at 675–676 eV), Th $4d_{3/2}$ (at 711–712 eV). More detailed information can be obtained from core-shell XPS spectra. Figure S5 compares the profiles of C 1s, O 1s, N 1s, P 2p, and Th 4f signals for the sorbents (HVP/NIP and HVP/IP) before and after Th(IV) sorption. These comparisons show that: (a) N 1s is roughly similar for the 4 samples, (b) Th 4f signal is not affected by the ion-templating (superposition for HVP/NIP and HVP/IP sorbents), (c) the sorption of thorium strongly perturbates the analysis of P 2p signal (which disappears); and (d) the signals most influenced by the mode of synthesis and the sorption of thorium concern essentially C 1s (probably those close to reactive phosphonic groups), and O 1s signals. Figures S6 and S7 offer a focus on the individual signals (after deconvolution) before and after Th(IV) sorption for HVP/IP and HVP/NIP, respectively. Table S3 summarizes the main components of the different deconvoluted bands (with their BEs and their relevant atomic fractions, AFs). The differences in the spectra between the two sorbents visible on C 1s, O 1s, and N 1s signals tends to confirm that the Th-templating affects the mode of reaction between the precursors. Hence, the relative fractions (more than their BEs) of some bonds change with ion-imprinting. For example, the AFs of bands at 286.20 eV (associated with C-P, C–C=O, C-N, C-N-C=O) and 287.8 eV (C=O bond) decrease with templating effect, contrary to the increased fraction for the signal at 284.8 eV (C–C, C–H). For O 1s signal, the largest variations are observed for the bands at 529.4 eV (O-P, and C-O bonds) and at 530.9 eV (O=P, H_2O): the first component increases with ion-imprinting, while the second tends to decrease. The repartition of the different components for N 1s signal slightly changes between amine and amide groups. It may be suggested that the ion-imprinting process contributes to preserve the reactive groups engaged in Th(IV) sorption during the final synthesis step; after elution of the template, these protected sites will be available for metal sorption (higher density of free reactive groups and more appropriate arrangement for adopting the spatial configuration of Th(IV) ionic species).

The sorption of Th(IV) introduces additional differences with their original form but also between the two types of metal-loaded sorbents. Considering the N 1s spectra, metal sorption affects essentially the N–H bond that disappears for both HVP/IP+Th and HVP/NIP+Th. The most marked differences can be observed for C 1s and O 1s signals. For C 1s signal, Th(IV) binding induces an increase of the AF of the bands at BE: 284.8 eV (C–C, and C–H) and BE: 289 eV (N-C=O), while the AF of other bands at BE: 286.2 eV and BE: ≈287.5 eV (which represent C in C=O, C-P, C-N, C–C=O, and C-N-C=O) tend to decrease (in terms of AF). For HVP/IP, the bands associated with O-P (at BE: 529.4 eV) and O=C/P-OH (at BE: 532.3 eV) tend to decrease, despite the formation of a

supplementary linkage between O-bearing functional group and Th (probably associated with the slight shift in BE from 532.3 to 532.6 eV). The band at 531 eV (assigned to O=P, O-P) shifts toward higher BE (at 531.4 eV). In the case of HVP/NIP, thorium sorption induces weaker shifts in binding energies and the variations in the AFs of the three bands are reversed (compared with ion-imprinted materials). The P 2p signal well-resolved in the as-produced sorbent, is strongly "denatured" after metal binding (impossibility to deconvolute the dispersed signal). The Th 4f signals are observed at the same binding energies for the two metal-loaded sorbents, close to BE: 334.25 eV and BE: 343.55 eV for Th $4f_{7/2}$ and Th $4f_{5/2}$, respectively. Though N-based ligand may contribute to thorium sorption, most of the changes (and the most intense) are associated with O-donor ligands (C=O, amide, and phosphonic acid moieties).

3.1.2.4. Elemental analysis and pH_{pzc}. Table S4 shows that elemental analysis is also slightly influenced by the mode of synthesis (impact of the presence of the template). The relative percentages of O, N, and P slightly increase with templating (traduced by increases of molar content in the range 0.7–1.25 mmol g^{-1}). These differences support the hypothesis that the synthesis route may be affected by the presence of the template. Monier and Abdel-Latif [63] designed an ion-imprinted resin based on functionalized carboxymethyl cellulose for U(VI) removal; the comparison of elemental analysis of the standard and ion-imprinted salicylaldehyde-grafted materials showed a relative decrease in N content.

The ion-templating weakly influences the pH_{pzc} of the sorbents (Fig. S8). The value is shifted from 5.47 to 5.60 with ion-imprinting. Below pH ≈5.5, the sorbents are protonated; associated with the increase of the pH. On the other hand, above pH ≈5.5, the pH of the solution tends to decrease, and the sorbent is progressively deprotonated. The curves are parallel to each other with a little shift toward (slightly) higher values for ion-imprinted sorbent. The surface acid-base behavior results from the cross effects of the different functional groups present at the surface of the sorbent; i.e., amide-type (pK_a: 6.57 for HMAA and 6.25 for MBA) and phosphonic acid-type (pK_a: 3.68 for VPA) [64]. The changes in their environment that occur during the synthesis process (which can be also influenced by the templating effect) may induce inductive and/or cooperative effects that, in turn, influence the final acid-base properties of the sorbents.

3.2. Study of sorption properties – Synthetic solutions

3.2.1. Effect of pH

The pH plays a role on both the speciation of metal ions and the surface charge of the sorbent, which, in turn, influence the possible interactions between the sorbent and the metal ions through attraction/repulsion and competition effects. Fig. 3 compares the sorption capacities for the two sorbents at room temperature (i.e., 294 ± 1 K) and at T: 323 ± 1 K in function of equilibrium pH. The pH-edge curves are characterized by a two-slopes shape: (a) in acidic solutions (pH_{eq} < 3–3.5) the sorption capacity increases almost linearly with the pH, and (b) at pH_{eq} > 3–3.5, the slope decreases with inversion. In acidic solutions, the pH increase limits the competition of protons; the progressive deprotonation of reactive groups contributes to the strong increase in thorium sorption. It is noteworthy that the "frontier" does not correspond to pH_{pzc} values (≈5.5). Moulin et al. [65] published a critical comparison of thorium speciation in aqueous solutions; they reported that thorium distribution profiles may significantly vary with data source. This may be due to different experimental conditions (such as background salt and concentrations). In strong acidic solution (i.e., pH below 1), thorium is mainly present in solution as free Th^{4+} (though some authors also document the presence of $Th(OH)^{3+}$, [66]). With pH increase, hydrolyzed species progressively appear in the solution: mostly as $Th(OH)^{3+}$, which is predominant at pH > 2 [65,66]. With further pH

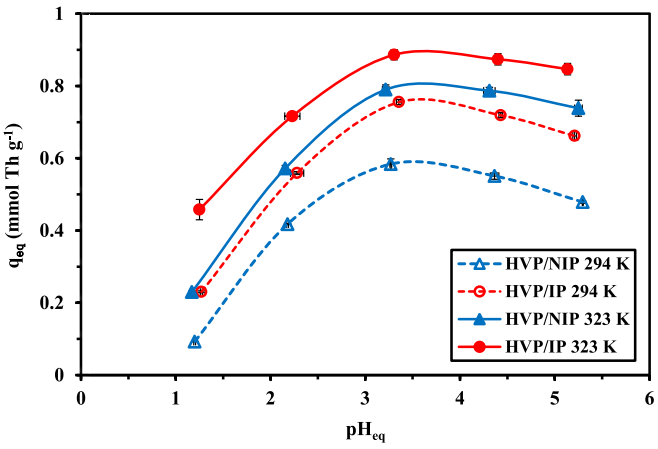

Fig. 3. Effect of pH on Th(IV) sorption using HVP-based sorbents at two temperatures (T: 294 ± 1 K or 323 ± 1 K; C_0: 0.224 mmol Th L^{-1}; Sorbent dose, SD: 0.5 g L^{-1}; v: 210 rpm; time: 48 h).

increase, the relative fractions of $Th(OH)_2^{2+}$ and $Th(OH)_3^{+}$ species progressively increase (their relative importance depends on literature source, [65,67]). Sasaki et al. [68] listed formation constants of thorium hydroxides; these values were averaged and used for drawing the speciation diagram of Th(IV) (at 1 mmol Th L^{-1} concentration, Figure S9); successive predominant species are Th^{4+} (pH below 2), $Th(OH)^{3+}$ (at pH 3), $Th(OH)_2^{2+}$ (at pH 4), $Th(OH)^{3+}$ (at pH 5), and $Th(OH)_4$ (at pH 6). More recently, Nisbet et al. [69] investigated the solubility (and speciation) of thorium at different temperatures. At 298 K, they only identified three species: (a) free Th^{4+} (alone until pH 2), (b) $Th(OH)_2^{2+}$ (alone at pH 4.5), and $Th(OH)_4^0$ (above pH 6); with mixed compositions in the relevant intermediary pH ranges. Depending on thorium concentration, precipitation phenomena can be observed at pH higher than 4–5. It is noteworthy that increasing the temperature significantly shifted the pH-distribution profiles toward lower pH (i.e., $Th(OH)_2^{2+}$ predominates at pH 2 for T: 373 K). Therefore, the changes in the sorption efficiency of the sorbents for Th(IV) binding (with slope breaking) can be correlated with both the progressive decrease of the protonation of reactive groups and the speciation of the metal through the formation of hydrolyzed species that may be less favorable to metal binding (especially highly hydrolyzed species, with lower positive charge and higher hydroxyl groups). At the highest pH values, the occurrence of precipitation phenomena may interfere with sorption process with misinterpretation of thorium removal (combined precipitation and sorption); to avoid this drawback, further studies are performed at pH 3.

The increase in the temperature improves sorption capacity for Th (IV): the sorption is endothermic. It is noteworthy that the endothermic effect is more marked for HVP/NIP, especially for the second section of the curves (pH higher than 3.5). Complementary information may be obtained from pH variation during the sorption (possible impact of speciation and precipitation, Figure S10) and from the evolution of the distribution ratio with pH (contribution of ion-exchange mechanisms, Figure S11). More detailed explanations are provided in Text S4 (in SI).

3.2.2. Uptake kinetics

The kinetic profiles for Th(IV) using HVP/NIP and HVP/IP show equilibrium contact times of roughly the same order of magnitude (Fig. 4): about 30 min for HVP/NIP and little lower for HVP/IP (i.e., ≈20 min). However, the benefits of ion-imprinting are more significant in terms of equilibrium sorption capacities. Consistently with Fig. 3, templating effect increases q_{eq} from 0.537 to 0.699 mmol Th g^{-1}.

Generally, sorption processes are kinetically controlled by diffusion mechanisms (including resistance to bulk, film, and intraparticle diffusion) and proper reaction rates (which may be approached using pseudo-

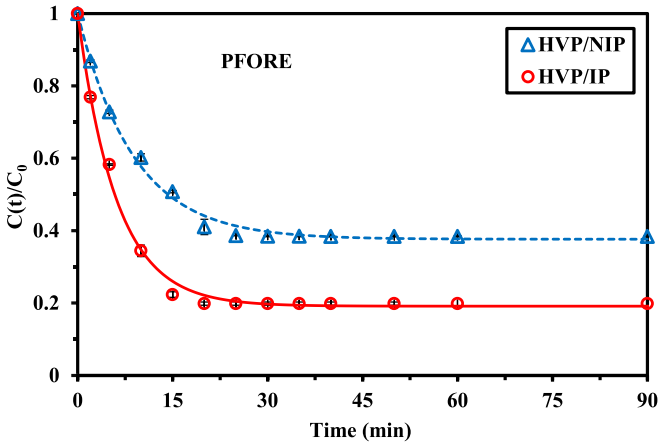

Fig. 4. Comparison of kinetic profiles for Th(IV) sorption using HVP-based sorbents – Modeling with pseudo-first order rate equation (PFORE) (pH_0: 3.02; C_0: 0.544 mmol Th L^{-1}; Sorbent dose, SD: 0.5 g L^{-1}; v: 210 rpm; T: 294 ± 1 K).

first order (PFORE) and pseudo-second order (PSORE) rate equations). Table 1 compares the modeling of kinetic profiles using the PFORE and PSORE fits with the so-called Crank equation (simplified modeling of resistance to intraparticle diffusion, RIDE).

From the general Langmuir equation kinetics (Eq. 1), Azizian [70] derived two equations that actually correspond to the conditions of so-called Lagergren equation (or pseudo-first-order rate equation, PFORE, Eq. 2) and pseudo-second order rate equation (PSORE, initially described by Blanchard, [71], Eq. 3) [72]:

$$\frac{d\theta}{dt} = k_a\left(C_0 - \frac{mq_m}{V}\theta\right)(1-\theta) - k_d\theta \quad (1)$$

$$\frac{dq_t}{dt} = k_1(q_e - q_t) \qquad \text{for } C_0 \gg \frac{m\,q_m\,\theta}{V} \quad (2)$$

$$\frac{dq_t}{dt} = k_2(q_e - q_t)^2 \qquad \text{for } C_0 \text{ of the same order than } \frac{m\,q_m\,\theta}{V} \quad (3)$$

with: m is the mass of sorbent, q_m the maximum sorption capacity of the sorbent, θ occupied fraction of sorption sites, and V the volume of solution.

Salvestrini [73] reported the misuse of the Langmuir equation for systems controlled by resistance to diffusion, and he proposed an alternative equation called Diffusion-Controlled Langmuir Kinetics (DCLK). Tran et al. [74] reminded that the PFORE requires careful attention regarding (a) the consistency between calculated sorption capacity at equilibrium ($q_{e,calc}$) and relevant experimental value ($q_{e,exp}$), and (b) that the model cannot appropriately describe the full range of the kinetics (being rather limited to the initial contact time, i.e., 20–30 min). The discrepancy in the values of equilibrium sorption capacities can be associated with the contribution of the boundary layer (for resistance to external diffusion) at the beginning of the kinetics.

Table 1
Th(IV) uptake kinetics for HVP/NIP and HVP/IP sorbents – Parameters of the models.

Model	Parameter	Unit	Sorbent	
			HVP/NIP	HVP/IP
Experimental	$q_{eq,exp.}$	mmol g^{-1}	0.537	0.699
PFORE	$q_{eq,1}$	mmol g^{-1}	0.544	0.705
	k_1	min^{-1}	0.113	0.164
	R^2	–	0.995	0.996
	AIC	–	−122	−120
PSORE	$q_{eq,2}$	mmol g^{-1}	0.599	0.763
	k_2	g $mmol^{-1}$ min^{-1}	0.279	0.335
	R^2	–	0.967	0.965
	AIC	–	−95	−87
RIDE	$D_e \times 10^{15}$	m^2 min^{-1}	8.78	5.62
	R^2	–	0.978	0.972
	AIC	–	−99	−89

The PFORE remarkably fits Th(IV) sorption kinetics (solid lines in Fig. 4). The fit of kinetics with PSORE is frequently associated in the literature with predominance of chemical sorption. However, Hubbe et al. [75] demonstrated that specific conditions must be fulfilled for validating this "short-cut"; alternatively, the mathematical fit only covers system controlled by the resistance to intraparticle diffusion. These conditions (such as invariability of metal concentration; i.e., infinite volume conditions) are not fulfilled herein. Figure S12 shows the dispersion of data in the zone of higher curvature (for PSORE and RIDE) and at the equilibrium (for PSORE). Table 1 also demonstrates that the calculated values for the equilibrium sorption capacities are remarkably close to experimental values (overestimation does not exceed 1.3 %); this is another proof that the PFORE allows finely simulating thorium sorption onto HVP-based sorbents. Consistently with equilibrium times, the apparent rate coefficient (i.e., k_1) slightly increases with ion-templating (from 0.113 to 0.164 min^{-1}). HVP sorbents exhibit higher apparent rate coefficient than alternative sorbents, especially for ion-imprinted material (extended discussion is available in Text S5, in SI). It is noteworthy that contrary to the current trend, Liang et al. [60] reported a decrease in the k_1 value after ion-imprinting. Similar decreasing trend is reported by Sharef et al. [76] for copper removal using a bio-based imprinted polymer.

3.2.3. *Sorption isotherms and thermodynamics*

The sorption isotherms plot the evolution of the sorption capacity in

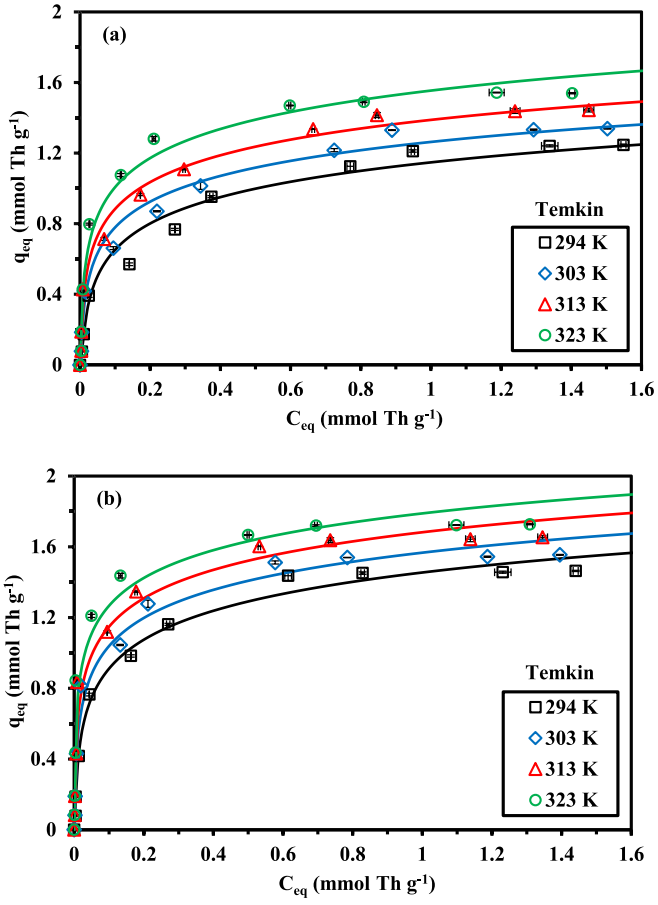

Fig. 5. Effect of temperature on Th(IV) sorption isotherms using HVP/NIP (a) and HVP/IP (b) – Modeling with Temkin equation (C_0: 0.043–2.18 mmol Th L^{-1}; pH_0: 3.01 ± 0.02; pH_{eq}: 3.18–3.35; SD: 0.5 g L^{-1}; time: 48 h; v: 210 rpm).

function of the residual adsorbate concentration (Fig. 5). The comparison of pH-effect curves at T: 294 K and 232 K, brought a first indication on the endothermic nature of Th(IV) sorption on HPV sorbents. Fig. 5 confirms these trends with the sorption isotherms shifting systematically towards higher sorption capacities with temperature increase. The profiles are characterized by a steep initial section followed by a progressive increase, and a quasi-saturation plateau. This type of shape disqualifies the Freundlich model for fitting experimental profiles (because of the power function-type of this model, contrary to the plateau/semi-plateau associated with other models). Langmuir equation describes the equilibrium distribution of the sorbate between the two phases assuming that the sorption occurs as a monolayer, without interaction between sorbed molecules and with constant sorption enthalpy (meaning homogeneous distribution of sorption sites with equivalent enthalpy of sorption). Another requisite is the complete reversibility of solute binding. Misak [77] demonstrated that the Langmuir equation cannot be applied to equilibrium driven by ion exchange mechanism (the mechanism ca be better considered as competitive adsorption between ion-exchanged solutes, which requires a modified version of the Langmuir equation, [77]). Herein, the sorption process may involve (depending on the pH and the reactive groups) ion-exchange mechanisms or complexation and chelation mechanisms. The use of the Langmuir equation is thus mathematically extended to conditions that do not perfectly fit the equation requisites. Tables 2 and 3 compare the fitting of experimental profiles with the different models for both HVP/NIP and HVP/IP at different temperatures. The statistical criteria (R^2 and AIC) show that in most cases, the Temkin equation best fits experimental data. In the case of Temkin equation, the adsorption enthalpy (contrary to Langmuir system) is not constant and varies linearly with surface coverage; this variation may be due to eventual interactions between sorbed sorbate molecules, and/or to heterogeneities of sorption sites [78].

The AIC is most relevant for evaluating the quality of the fit since this criterion also considers the number of adjustable parameters. In Fig. 5, the solid lines represent the fitting of sorption isotherms with Temkin equation; Figures S13-16 show the sorption isotherms fitted with the Langmuir, Langmuir Dual Site, Sips, and D-R equations (Tables S5a and S5b show the parameters for Freundlich and Langmuir Dual Sites equations). Considering Temkin model, the a_T parameter slightly increases with temperature (from 10,367 to 11,855 L mmol^{-1}) for HVP-IP, while for the reference material the parameter strongly increases with temperature (being tripled between 294 K and 323 K) but remains much lower (below 694 L mmol^{-1}) than for ion-imprinted sorbent. The energetic parameter of the Temkin equation (i.e., b_T) does not vary with temperature for HVP/IP (11638 ± 302 J kg^{-1} mol^{-2}) contrary to HVP/NIP, where b_T progressively increases (with much lower values, from 475 to 2671 J kg^{-1} mol^{-2}). The ion-templating effect strongly impacts sorption performances and energy dimension of the sorption process. The sorption energy (E_T, derived from Temkin modeling) hardly varies for HVP/IP (6.95 ± 0.13 kJ mol^{-1}), while for HVP/NIP E_T continuously decreases with increasing temperature from 9.17 to 7.33 kJ mol^{-1}. The ion-templating decreases the energy to provide for thorium binding.

Despite the poorer statistical quality of the Langmuir equation for fitting sorption isotherms, the model can help figuring the beneficial effect on ion imprinting. The experimental sorption capacities ($q_{m,exp}$) are consistent with the maximum Langmuir sorption capacities ($q_{m,L}$), which increase with temperature. The Langmuir equation supposes that the sorption occurs as a monolayer without interactions between sorbed molecules and with homogeneous distribution of sorption energies at the surface. The Langmuir Dual Site model has been designed for simulating sorbents with two types of reactive groups having different sorption energies but obeying to Langmuir hypotheses. This alternative model improves the quality of the fit (compared to Langmuir equation) for HVP/NIP, while the fitting is not improved for HVP/IP; this is another evidence that the ion-templating changes the sorption mechanisms with different contributions and changes in the configuration of the reactive groups. The affinity coefficient (i.e., b_L) increases with temperature as a confirmation of the endothermic sorption of Th(IV): for HVP/NIP, b_T increases from 6.12 to 35.2 L mmol^{-1}; these values are much lower than those obtained for HVP/IP (i.e., 21.3 to 123 L mmol^{-1}). As expected by design, the ion-imprinting significantly increases the affinity of HVP sorbent for Th(IV). Liang et al. [60] also observed an increase (3-folds) of the affinity constant for ion-imprinted polymer. Table S6 demonstrates that the properties (not only sorption capacity but also kinetics) of HVP/IP for thorium recovery are globally comparable to the best sorbents reported in the literature, featuring promising sorbent for Th(IV) recovery from dilute solutions (more detailed discussion in available as Text S6 in SI).

The calculation of thermodynamic parameters is reported in detail in Text S7 (based on the method described by Tran et al. [79]). Figure S17 displays the plots of the van't Hoff equation for the two sorbents. Thermodynamic parameters are compiled in Table S7. It is noteworthy that the values are remarkably similar for the two materials: the ion-imprinting does not significantly affect the value of enthalpy (around 46 kJ mol^{-1}), while the entropy change hardly increases (by 6 %) with the effect of ion-templating. Despite the significantly enhanced affinity of HVP/IP, the thermodynamic parameters are minimally affected by ion-imprinting. Sharef et al. [76] observed the significant increase of thermodynamic parameters for copper sorption onto bio-based polymer when ion-templating is applied. Ion-imprinting also increased the values of thermodynamic parameters in the case of uranium recovery using amino-phenolic functionalized chitosan [80]. Table S8 compares the thermodynamic parameters for thorium sorbents. HVP-based sorbents show among the highest values for the three parameters (being only overpassed by the chitosan/Al_2O_3 system, [81]).

Table 2
Th(IV) sorption isotherms for HVP-NIP sorbent – Parameters of the models.

Model	Parameter	Unit	Temperature (K)			
			294	303	313	323
Exp.	$q_{m,exp}$	mmol g^{-1}	1.25	1.34	1.44	1.54
Langmuir	$q_{m,L}$	mmol g^{-1}	1.37	1.40	1.48	1.52
	b_L	L mmol^{-1}	6.12	10.2	14.4	35.2
	R^2	–	0.978	0.971	0.974	0.986
	AIC	–	−51	−46	−45	−53
Sips	$q_{m,S}$	mmol g^{-1}	**1.86**	1.91	1.86	1.62
	b_S	(L mmol^{-1})$^{1/bS}$	**1.72**	2.06	3.08	14.2
	n_S	–	**1.66**	1.82	1.73	1.25
	R^2	–	**0.989**	0.988	0.989	0.991
	AIC	–	**−57**	−54	−54	−53
Temkin	a_T	L mmol^{-1}	207.6	**407.6**	**564.4**	693.6
	b_T	J kg^{-1} mol^{-2}	11,371	**11,996**	**11,878**	11,308
	E_T	kJ mol^{-1}	9.17	**8.96**	**8.23**	7.33
	R^2	–	0.981	**0.987**	**0.990**	0.987
	AIC	–	−55	**−57**	**−59**	−54
D-R	$q_{m,D-R}$	mmol g^{-1}	1.23	1.30	1.42	**1.56**
	$k_{D-R}\times10^8$	mol^2 kJ^{-2}	2.09	1.36	1.11	**0.849**
	E_{D-R}	kJ mol^{-1}	6.92	8.56	9.48	**10.8**
	R^2	–	0.965	0.967	0.976	**0.991**
	AIC	–	−47	−47	−49	**−56**

3.2.4. Sorption mechanisms

The data from FTIR and XPS analyses show the contribution of both O-bearing groups (OH, C=O and P=O from HMAA, VPA and MBA) and N-bearing groups (amides from HMAA and MBA) to metal binding. The tautomerization reactions (displayed in Scheme 2) contribute to the modulation of reactive groups like formation of hydroxyl groups (from carbonyl moieties of acrylamide) or attachment of two hydroxyl groups to amine moiety, which all contribute to metal binding. The slope analysis of the plots of $\log_{10} D$ against pH_{eq} suggests the possible crossed contributions of both ionic exchange and chelation mechanisms in the

Table 3
Th(IV) sorption isotherms for HVP-IP sorbent – Parameters of the models.

Model	Parameter	Unit	Temperature (K)			
			294	303	313	323
Exp.	$q_{m,exp}$	mmol g^{-1}	1.46	1.55	1.65	1.73
Langmuir	$q_{m,L}$	mmo g^{-1}	1.48	1.51	1.59	1.66
	b_L	L $mmol^{-1}$	21.3	47.7	72.9	123
	R^2	–	0.983	0.972	0.961	0.961
	AIC	–	−51	−45	−40	−39
Sips	$q_{m,S}$	mmol g^{-1}	1.65	1.69	1.79	1.79
	b_S	$(L\ mmol^{-1})^{1/bS}$	6.81	9.63	10.6	20.8
	n_S	–	1.38	1.45	1.51	1.41
	R^2	–	0.990	0.982	0.972	0.969
	AIC	–	−54	−46	−39	−37
Temkin	a_T	L $mmol^{-1}$	**10,367**	**10,997**	**11,230**	11,855
	b_T	J kg^{-1} mol^{-2}	**475**	**929**	**1414**	2671
	E_T	kJ mol^{-1}	**7.08**	**7.08**	**6.79**	6.86
	R^2	–	**0.992**	**0.985**	**0.975**	0.962
	AIC	–	**−60**	**−52**	**−45**	−39
D-R	$q_{m,D-R}$	mmol g^{-1}	1.48	1.56	1.66	**1.76**
	$k_{D-R}\times10^8$	mol^2 kJ^{-2}	1.24	0.874	0.714	**0.555**
	E_{D-R}	kJ mol^{-1}	9.00	10.7	11.8	**13.4**
	R^2	–	0.989	0.981	0.971	**0.967**
	AIC	–	−56	−49	−43	**−40**

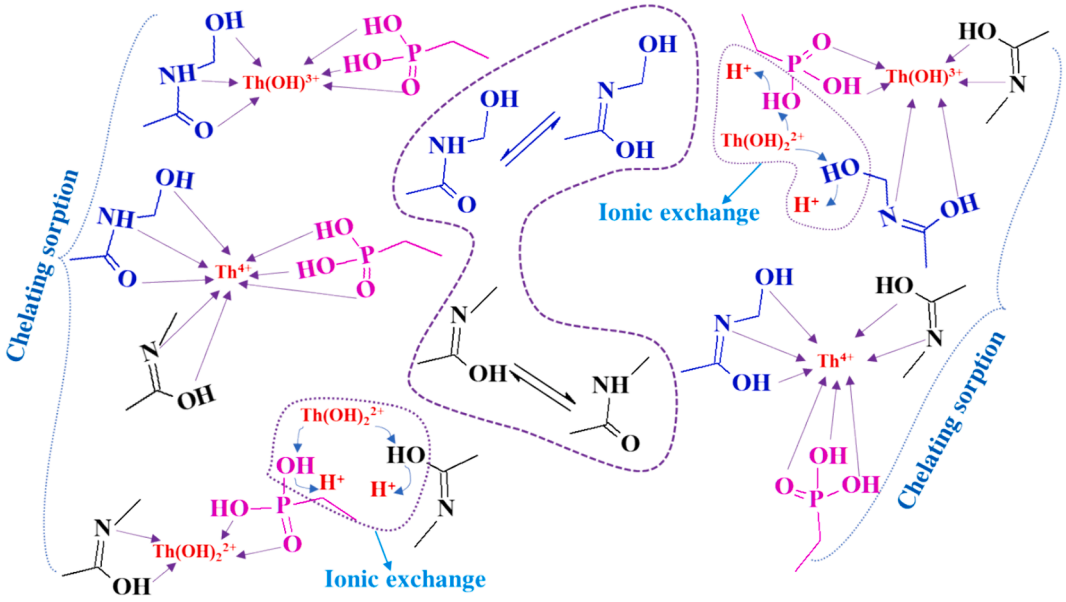

Scheme 2. Suggested modes of interaction of thorium with HVP/IP.

interaction of the sorbent with thorium. The pHpzc (close to 5.5) can be correlated with the optimum pH found close to 4, meaning that the partial protonation of the sorbent facilitates metal binding. On the other hand, $Th(OH)_2^{2+}$ is the predominant thorium species under these optimum conditions; though some other species coexist (i.e., Th^{4+} and $Th(OH)^{3+}$). The tautomerization and the partial charge on either N and O opens the possibility to sorb cationic thorium species through proton exchange or by chelation on negatively charged reactive groups. Scheme 2 shows the expected interaction modes of cationic thorium species with the functional groups; the main interaction occurs through hydroxyls/O-bearing groups and amines in either tautomerized (right side) or non-tautomerized (left part) sorbent.

3.2.5. *Metal desorption and sorbent reuse*

Evaluating metal desorption and sorbent recycling are important steps in the design of a new sorbent. Several eluents were tested, including ethanol, neutral solutions (1 M NaCl and 1 M $NaNO_3$), alkaline solutions (0.5 M NaOH and 1 M Na_2CO_3), acid solution (0.3 M HNO_3), and a complexing solution (0.5 M EDTA) (Fig. S18a,b). The kinetics are commented in text S8 (in Supplementary Information). Playing with extreme pH values allows reversing metal binding due to the competition of protons (acid eluent) and/or speciation impact (acid and alkaline eluents). Based on these results, 0.3 M HNO_3 solution is selected for further studies since this eluent allows full release of thorium in shorter contact time. The first target of desorption step consists of the recovery of the metal bound to the sorbent; however, for the competitiveness of the process (especially for further valorization of the metal), the concentrating effect of the desorption step is another important requisite (Fig. S18c,d). In this preliminary optimization of the desorption process, 0.3 M HNO_3 solution reaches complete desorption of thorium with a maximum sorbent dose of 3.33 g L^{-1}. Under these conditions, full desorption is achieved in ≈30 min with HVP/IP and ≈40 min with HVP/IP. Considering the double constraint of concentrating effect and full recovery of thorium; the best conditions correspond to sorbent dose: 3.33 g L^{-1} with CF: 4.12 and 5.46 for HVP/NIP and HVP/IP, respectively. Therefore, the ion imprinting allows both a faster desorption and

more efficient desorption combined with higher concentrating effect.

The next step in the evaluation of the performances of the sorbents concerns the capacity to reuse the sorbents. Fig. 6 compares for similar experimental procedures, the sorption and desorption properties of HVP/NIP and HVP/IP for ten successive sorption and desorption cycles. It is remarkable that thorium can be fully desorbed along the 10 cycles. It is also noticeable that the variation is negligible in terms of sorption efficiency. Indeed, at the tenth cycle, the loss in sorption performance does not exceed 3.6 % for HVP/NIP and even lower (i.e., 2 %) for HVP/IP. The two sorbents exhibit remarkable stability at recycling. The benefit of ion-imprinting is essentially observable in terms of kinetics of desorption and concentrating effect.

To compare the desorption properties of alternative sorbents, Table S9 reports global performances (choice of eluent, desorption efficiency and loss of performance at recycling). Though some other systems allow complete thorium desorption [82–84], HVP sorbents show outstanding stability in terms of sorption stability (comparable to the properties reported by Hamza et al. [84,85]). This is another merit of HVP materials that confirms their promising performances for thorium recovery from dilute effluents at mild acidity.

3.2.6. *Sorption from multicomponent solutions – Selectivity*

The complexity of real effluents that contain a wide diversity of metal ions (which may be competitor in the sorption process) may strongly impact the evaluation of the potential of new sorbents. To evaluate the selectivity of HVP sorbents, multicomponent solutions (at equimolar concentration, 1 mmol L^{-1}) were tested for metal sorption at different pH values. Competitor metals have been selected for the diversity of their physicochemical characteristics (divalent/trivalent cations, alkaline earth elements, base metals, members of different class of metals according HSAB principle, [37]) and/or for their coexistence in thorium-bearing mining effluents (such as uranium). Fig. 7 compares the pH-edge curves for sorption capacities for HPV sorbents. The reference material (i.e., HVP/NIP) shows a preference for U and Th in acidic solutions (pH_0 3) according: Th > U > Fe≈Zn≈Al > Pb≈Cd > Ca; at mild acidity, the ranking is slightly modified: Th > U≈Fe≈Zn≈Al > Ca≈Cd > Pb. The ion-imprinting reinforces the preference of the sorbent for thorium (increased sorption capacity and larger separation of the curves). Hence, at pH_0 3, ion-templating procedure increases sorption capacity from 0.472 to 0.671 mmol Th g^{-1}, and the sorption capacities are ranked according: Th ≫ U ≫ Fe > Zn > Pb > Ca > Cd > Al. Figure S19 compares the cumulative sorption capacities. HVP-NIP tends to show a higher total sorption capacity than HVP/IP because of lower selectivity and sorption of competitor metal ions (in place to thorium); Text S9 (in supplementary Information) provides deeper discussion

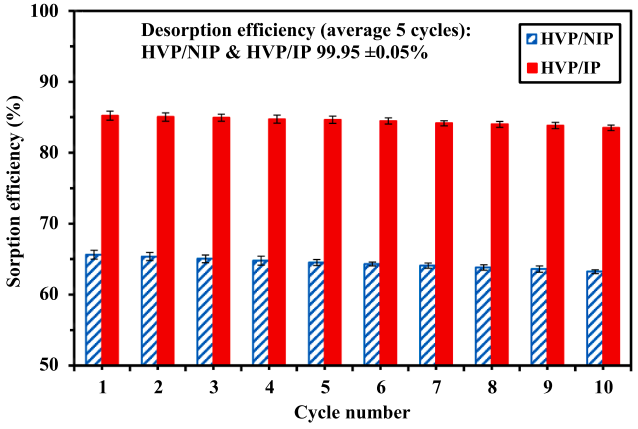

Fig. 6. Sorption and desorption efficiencies for Th(IV) recovery using HVP-based sorbents for 10 successive cycles (Th-loaded sorbents collected from uptake kinetics (with SD: 0.5 g L^{-1}); desorption using 0.3 M HNO_3 solution, SD: 1.33 g L^{-1}; time 2 h; v: 210 rpm; T: 294 ± 1 K).

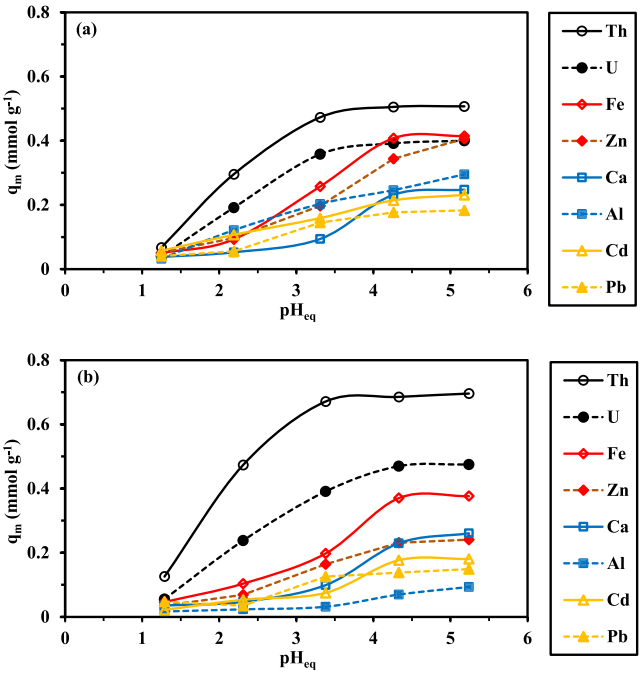

Fig. 7. Effect of pH_{eq} on sorption capacity for selected metal ions using HVP/NIP (a) and HVP/IP (b) (C_0: 1 mmol L^{-1}; SD: 1 g L^{-1}; time: 24 h; v: 210 rpm; T: 294 ± 1 K; $SC_{Th/Th}$ = 1, as reference).

using other indicators.

The selectivity coefficient $SC_{Th/metal}$ offers another view of the preference of the sorbents for thorium:

$$SC_{Th/metal} = \frac{D_{Th}}{D_{metal}} = \frac{q_{eq,Th} \times C_{eq,metal}}{C_{eq,Th} \times q_{eq,metal}} \quad (4)$$

Fig. 8 shows the $SC_{Th/metal}$ values at different pH_{eq} for HVP/NIP and HVP/IP. The sorbents exhibit higher selectivity when pH_{eq} ranges between 2.0 and 3.4 and the highest selectivity are recorded against Ca > Pb > Cd≈Zn≈Al for HVP/NIP and Al ≫ Ca≈Pb≈Cd for HVP/IP. The ion-imprinting strongly increases the selectivity for Th against competitor metals (apart from U(VI)): the $SC_{Th/metal}$ value remains below 8.2 for reference HVP/NIP; with ion-templating the SC values may reach up to 37–59 (in the case of Al).

According HSAB principles (Pearson's rules, [37]), hard acids (metals) preferentially bind to hard base (ligands) (and reciprocally, soft acids preferentially react with soft bases). Among selected metals, U(VI), Th(IV), Ca(II), Al(III), and Fe(III) are hard acids, Cd(II) and Zn(II) are borderline metals, while Pb(II) is considered a soft metal (sometimes classified as the softer of borderline metals, [86]). O-bearing ligands (and N-bearing ligands to a lesser extent) are considered hard base. The preference order does not strictly obey the theoretical ranking; at least concerning the "position" of Zn(II) in the orders of preferences. The ion-imprinting strongly improves the affinity of the sorbent for U(VI) and Th(IV) (especially at pH<3.5), and the order of selectivity is closer to the expected ranking (i.e., Th > U > Fe > Ca,Zn > Cd > Pb > Al), with the remarkable anomaly of Al that shows the lowest affinity for HVP/IP. The effects of metal speciation under variable pH conditions may superpose to the affinities oriented by HSAB principles to modulate the effective selectivity. Table S10 reports physicochemical properties of selected metal ions and compares the sorption capacities obtained at pH 3 for imprinted and non-imprinted HVP sorbents. It is noteworthy that the metal ions having the octahedron configuration are those having the sorption capacity the most depreciated. It is also remarkable observing that the ranking in sorption and the analysis of the beneficial effect of ion-templating cannot be strictly correlated with the values of the different physicochemical criteria reported in Table S10. However,

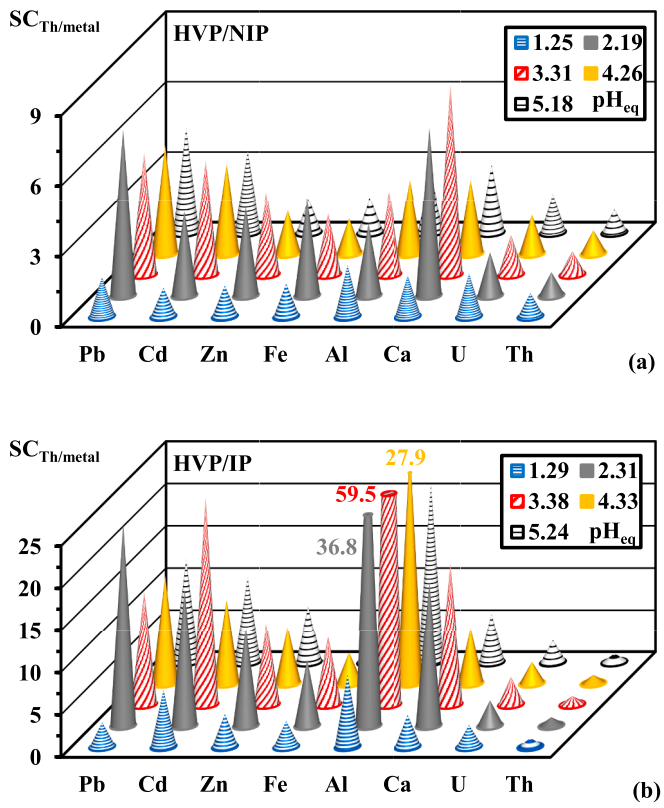

Fig. 8. Comparison of selectivity coefficients ($SC_{Th/metal}$) for Th recovery from multicomponent equimolar solutions using HVP/NIP (a) and HVP/IP (b) sorbents – Effect of pH (C_0: 1 mmol L^{-1}; SD: 1 g L^{-1}; time: 24 h; v: 210 rpm; T: 294 ± 1 K; $SC_{Th/Th} = 1$, as reference).

Figure S20 shows that for reference material (i.e., HVP/NIP) the sorption capacity correlates with the solution-phase electronegativity (χ_{aq}, as defined by Li et al., [87]; U(VI) is not shown since the relevant χ_{aq} value is not available) for base metals; while the preference for thorium is marked by the strong increase of the sorption capacity. On the other hand, the ion-templating hardly affects the plots for Ca, Pb, Zn, and Fe (data are linearly aligned with correlation line close to that of HVP/NIP), while the sorption of both Cd and Al is significantly reduced.

The proper effect of ion-imprinting is controlled by a diversity of factors: (a) the cage effect (the polymerization around ion-template creates a cage with a recognition pathway for the target metal in terms of size sieving), and (b) the arrangement of ligands for appropriate chelate organization.

Table S11 compares the separation properties of different sorbents for thorium in the presence of uranium, rare earths, and base metals; however, most of the work was dedicated to the separation of U and Th from REEs. Some trends are outlined in Text S9.

3.2.7. *Ion-imprinting benefits*

Selambakkanuu et al. [42] investigated the selective recovery of thorium (against uranyl) using ion imprinted nonwoven fabric grafted with poly(2-dimethylaminoethyl methacrylate). They optimized the synthesis of the material by variation of the proportions of precursors (and grafting yield), reaction and crosslinking temperatures, ion-imprinting concentration, and irradiation dose. They reported higher selectivity for templated material and they explained that the cavity arrangement was favorable to thorium binding due to size and coordination geometry, whereas for non-imprinted material the synthesis produced random distribution of ligand functionalities (with poorer affinity) [88]. Therefore, uranium sorption by the non-imprinted sorbent was enhanced by opposition to thorium. Generally, sorption selectivity for thorium was favored at low metal concentration, decreased with the level of crosslinking (lower availability and flexibility), while increasing the concentration of thorium during the imprinting procedure hardly changed selectivity. It is anticipated that the presence of thorium during the synthesis of HVP/IP plays on the arrangement of precursors' moieties, which, in turn, leads to the formation of a spatial arrangement of functional groups that is favorable to thorium access and reaction (size and geometric interaction with functional groups [42], orientation of reactive groups [89]).

Herein, the ion-imprinting did not significantly affect the influence of the pH on Th(IV) sorption, the uptake kinetics were slightly enhanced. Metal desorption and sorbent recycling do not show significant differences in terms of stability of performances. The most significant benefits concern the increase in maximum sorption capacities and sorbent affinity. It is noteworthy that increasing the temperature tends to modulate and moderate the beneficial effect of ion-imprinting. Another expected beneficial effect of ion-templating deals with the selectivity of the sorbent for target metal. To better measure this enhancement, it is possible defining the β-coefficient:

$$\beta = \frac{\left(SC_{Th/metal}\right)_{HVP/IP}}{\left(SC_{Th/metal}\right)_{HVP/NIP}} \quad (5)$$

The β-coefficient is favored by acidic solutions (i.e., pH_0: 1–3) (Figure S21a). In addition; the highest enhancements follow the trend: Al(III) (up to 16.8) > Cd(II) (4.5) > Zn(II)≈Pb(II)≈Ca(II)≈Fe(III) > U(VI) (except at pH_0 1.01, where the ion-imprinting strongly increases the selectivity for thorium, though with low relative sorption capacities). Table S12 reports some data collected from literature on the improvement of sorption selectivity for thorium against competitor metal ions associated with ion-templating. Other panels in Figure S21 confirm the singularity of Th(IV) and U(VI) against other metal ions (as discussed in Text S10, in Supplementary Information).

The characterization of the sorbents both chemically (FTIR and XPS) and physically (textural properties) demonstrated that the ion-imprinting introduces detectable changes in the structure of the sorbent. This makes profit of the flexibility brought by MBA, which helps in adopting favorable cavity for thorium ion (during the synthesis); protected reactive groups (during polymerization) also contributes to adopting a favorable geometry for binding thorium. This may be correlated with higher sorption capacities (greater availability of reactive groups), but also faster kinetics (easier accessibility). The affinity of HVP/IP for thorium is substantially increased (Langmuir coefficient), consistently with the Temkin energy of sorption. The ion-imprinting does not change the stability (at recycling) of the sorbent but improves the desorption kinetics (consistently with sorption kinetics; due to higher availability and accessibility of reactive groups in favorable arrangement). The higher sorption capacity of ion-imprinted sorbent, in turn, enhances the concentrating effect (sorption/desorption operations).

The preference for Th(IV) and U(VI) over competitor ions is partially driven by the HSAB theory [37]. Th(IV) and U(VI) are hard acids (as are Ca(II), Al(III), and Fe(III)), which have greater affinity for complexation with hard bases (such as those reactive groups hold by HVP sorbents; i.e. O- and N-bearing groups such as acrylamide moieties, phosphonate and hydroxyl groups, as shown by FTIR and XPS characterization, which were illustrated in Scheme 2). Therefore, it is logical observing that HVP sorbents have poor affinity for metal ions such as Pb(II), Zn(II) and Cd(II) (which are classified among borderline or soft metal ions). However, the contribution of ion-exchange mechanisms can introduce some variations in the expected order of preference for competitor ions particularly. Hence, Al(III), despite being a hard acid that shows poor affinity for HVP sorbents, leaves the trend followed by other hard acids. This could be due to differences in the hydrolysis of metal ions (linked with their pK_s and pK_a values). The modulations introduced by pH may be also associated with tautomerization effects (indicated in Scheme 2). In

addition, the contribution of ion-exchange mechanisms may also affect the possibility to correlate the sorption properties with intrinsic properties since the relative contributions between chelation/complexation and ion exchange binding modes may vary with both pH and the nature of metal ions.

The ion-imprinting slightly enhances the selectivity for Th(IV) against U(VI) due to the template effect that favors the arrangement of reactive groups for binding Th(IV), and also because of the better availability of reactive groups for the metal ion (because the reactive sites are protected by bound thorium during the synthesis and become free after metal elution). The relative decrease in sorption capacities for competitor metal ions (except U(VI)) in the case of ion-imprinted material is directly correlated with the stronger sorption of Th(IV) that reduces the number of reactive groups available for the binding of competitor ions. Uranyl shows an intermediary behavior: higher sorption capacities and selectivity coefficients compared with other competitor ions, the sorbents have a marked preference for Th(IV). It is noteworthy that the ionic radius (r_p) of uranyl ions (i.e., 2.8 Å) is much larger than the r_p value for Th(IV) (i.e., 1 Å).

3.3. Application to thorium recovery from industrial effluent

3.3.1. Ore leaching and metal precipitation with pH control

Table S13 reports the composition of the leachate and the leaching yield for selected metals and metalloid. The leachate is characterized by huge amounts of aluminum and iron (up to 13.8 and 7.16 g L^{-1}, respectively); i.e., much higher concentrations than those observed for target metals (i.e., U, Ga, and Th, at 92.5, 10.5, and 68.9 mg L^{-1}, respectively). This huge excess of competitor metals may have a strong impact on the capacity of the sorbent to catch target metal ions. To evaluate the interest of pretreating the leachate (and reduce this competition effect), the leachate was controlled at different pH values using NH_3 and/or HCl solutions. Metal precipitation occurs at pH above 3 (Table S13). The analysis of the precipitation of metals must consider the dual objective of reducing the residual concentrations of Al and Fe with minimization of the loss of valuable metals. Figure S22 shows that at pH 1, metal precipitation does not exceed 7.5 % for Si (less than 3 % for U and Th). With increasing the pH_0 up to 3, metal/metalloid loss reaches 13–15 % for Si and Ga, between 2.8 % and 7.2 % for Na, Fe, Al, and Mn, while U and Th losses remain below 5 %. At pH_0 4, most of iron is strongly precipitated (about 94 %) but aluminum loss does not exceed 28 % (14–15 % for U and Th). It is necessary adjusting pH_0 to 5 to remove almost quantitatively Al (99 %) and Fe (98 %); target valuable metals (i.e.; Ga, U, and Th) remain relatively stable (precipitation yields remain below 25 %).

3.3.2. Treatment of leachates by sorption on HVP/NIP and HVP/IP

Due to substantial precipitation and co-precipitation phenomena (especially for pH_0 above 3), the data for sorption tests were calculated based on the effective initial concentrations of the metals after precipitation. Fig. 9 compares the sorption efficiencies at different pH values for selected metals with HVP/IP and HVP/NIP sorbents. As expected, metal sorption increases with the pH and HVP/IP is slightly better than HVP/NIP. It is necessary working at pH 3 and higher to achieve the most significant levels of recovery of target valuable metals. At pH ≈4 and ≈5, thorium sorption is almost quantitative (higher than 97 %) close to 83–95 % for uranium with HVP/IP (lower values are attained with non-imprinted material). Gallium is only recovered at 58–75 %; it is noteworthy that at high pH value, Si is also significantly sorbed (48–65 %); meaning unexpected recovery. These data are converted in selectivity coefficients ($SC_{Th/metal}$, Figure S23). The highest values are achieved at pH ≈4 and ≈5, with significant improvement for ion-imprinted material (much larger amplitude): the sorbent is more selective for Th against Al and Na (SC values in the range 219–336 for HVP/NIP and up to 1583–1885 for HVP/IP). It is noteworthy that the reference material (HVP/NIP) has poor selectivity for Th against U (0.44–2.55), while the

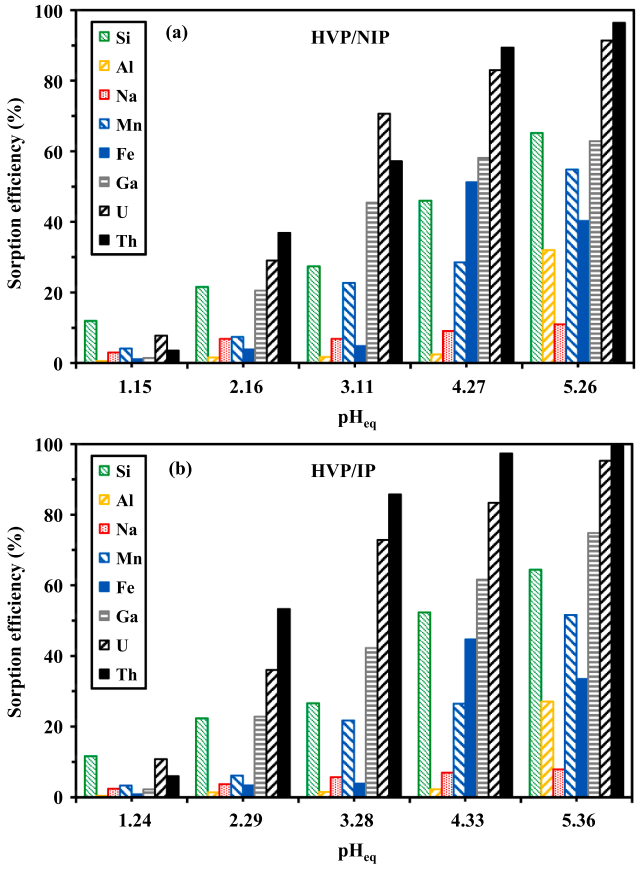

Fig. 9. Sorption efficiency for selected metals in the processing of leachates (calculations made after correction of the effective concentrations due to precipitation yields at the different pH values; SD: 2 g L^{-1}; time: 10 h; T: 294 ± 1 K; v: 210 rpm).

ion-imprinting improves the separation: $SC_{Th/U}$ increases from 0.52 to 8.01 with the increase of the pH. Under these experimental conditions the highest selectivity is reported at pH_0 5 for HVP/NIP according: Na ≫ Al ≫ Fe ≫ Mn > Ga > Si > U. For the ion-imprinted sorbent, the selectivity coefficient follows globally the same trend, it decreases according the ranking: Na ≫ Al ≫ Fe ≫ Mn > Si > Ga > U (with much higher values).

The templating strategy improves the separation properties of HVP material. This enhancement can be readily measured comparing the φ(metal) coefficients (Figure S24):

$$\varphi(metal) = \frac{D(metal)_{HVP/IP}}{D(metal)_{HVP/NIP}} \quad (6)$$

For most of the investigated metals (and metalloid; Si, Al, Na, Mn, and Fe), the value of φ-coefficient remains around (or below) the unity, regardless of the pH. This means that the ion-templating has a negligible effect (or even a slight depreciating effect) on their recovery from real effluent. This can probably be explained by the preferential binding of Th that limits the availability of reactive groups for these competitor ions. On the other hand, the ion-imprinting slightly enhances the recovery of Ga and U, especially at pH_0 5. However, the most significant impact is logically observed for thorium: the Th ion-imprinting drastically favors its recovery, especially at pH_0 3 and above: φ-coefficient is found close to 4.4 at pH_0 3–4 and increases up to 6 when the pH_0 reaches 5. The target of ion-imprinting by building the polymer across Th^{4+} ion is clearly reached: the organization of the sorbent polymer improves the selective recovery of thorium from complex solution. It is noteworthy that the cumulative sorption capacity (not shown) increases with the pH and reaches a maximum close to 15.3 mmol/g for HVP/NIP and only

12.8 mmol/g for HVP/IP at pH_0 3. The greater selectivity of the ion-imprinted sorbent for Th induces a loss in cumulative sorption capacity by almost 20 % (mainly due to reduced sorption of base metals, including alkaline and alkali-earth metals).

4. Conclusion

The challenge of successfully recovering thorium from complex effluents has been successfully met with the double strategy of (a) synthesizing a sorbent bearing phosphonate groups and carbonyl/amide groups, and (b) integrating an ion-imprinting step in the synthesis. This successful strategy allowed producing a stable sorbent (good recycling performance for 10 successive cycles) with fast sorption kinetics (equilibrium reached in 20 min), remarkable sorption capacity (up to 1.46 mmol Th g^{-1}, with endothermic behavior), high selectivity against base metals (and uranium to a certain extent). Preliminary results (obtained with multicomponent equimolar synthetic solutions) were confirmed in the treatment of complex effluent (collected after pre-treatment of acidic leaching of ore). The recovery efficiency reached up to 60–85 % for Th, U and Ga (under selected experimental conditions, at pH 3), despite the presence of large excess of competitor base metals.

The ion-imprinting does not affect pH influence, slightly improves the kinetic behavior and sorption capacity. The most significant impact of templating strategy concerns the significant improvement of the selectivity of the sorbent for thorium. This enhancement is more marked in acidic environment. Ion-imprinted HVP sorbent shows a good compromise in terms of kinetics, maximum sorption capacity, desorption efficiency (and recycling performance) and selectivity for thorium against other sorbents (including those materials adopting templating strategy). Though HVP/IP shows a good selectivity for base metals, it is noteworthy that the selectivity against uranium is less marked than for some other ion-imprinted materials.

Future development should focus on the conditioning of the material. This study was carried out in batch with micron-size sorbents for the characterization of mechanisms and performances. However, this conditioning is poorly adapted for large scale applications and it will be necessary investigating alternative solutions for facilitating the large-scale application of HVP/IP-based materials. In continuously stirred tank reactor, the solution may consist in agglomerating the materials (with a possible loss in diffusion properties) [90], or incorporating magnetite nanoparticles (for easy solid/liquid separation, but at the expense of a loss in the mass density of reactive groups). The application in fixed-bed columns (preferred for large scale application) is not possible with so thin particles (head loss pressure [91], blockage phenomena). To prevent these drawbacks, the agglomeration of particles [90] or their encapsulation in a porous matrix [92] (with possible diffusional constraints) may represent a solution; however, the most attractive method would consist in depositing the material on spherical porous materials [93] or using spheronization process (by extrusion [94], or by direct synthesis process such as dissolution-regeneration [95], suspension polymerization [96], or emulsion process [97]).

CRediT authorship contribution statement

Mengjie Zhao: Visualization, Formal analysis. **Amr Fouda:** Visualization, Formal analysis. **Khalid A.M. Salih:** Software, Investigation. **Eric Guibal:** Writing – review & editing, Writing – original draft, Software, Investigation, Data curation, Conceptualization. **Yuezhou Wei:** Project administration, Funding acquisition. **Shunyan Ning:** Validation, Funding acquisition. **Mohammed F. Hamza:** Writing – review & editing, Supervision, Resources, Methodology, Data curation. **Saly R. El Dakkony:** Methodology, Formal analysis.

Declaration of competing interest

The authors declare that they have no known competing financial interests or personal relationships that could have appeared to influence the work reported in this paper.

Data availability

Data will be made available on request.

Acknowledgements

Authors acknowledge the support from the National Natural Science Foundation of China (Grant No. 22350710186, U23B20167), and the National Key R&D Program of China for the project (2022YFB3506100).

Appendix A. Supplementary material

Supplementary data to this article can be found online at https://doi.org/10.1016/j.cej.2024.154045.

References

[1] "Agency for Toxic Substances and Disease Registry (US)", Toxicological Profile for Thorium. Atlanta (GA): Agency for Toxic Substances and Disease Registry (US); 2019 Sep. Chapter 2, Health Effects. Available from: https://www.ncbi.nlm.nih.gov/books/NBK591331/, U.S. Department of health and Human Services, Atlanta (GA), USA, 2019, 203 pp.
[2] K.S. Patel, S. Sharma, J.P. Maity, P. Martin-Ramos, Z. Fiket, P. Bhattacharya, Y. Zhu, Occurrence of uranium, thorium and rare earth elements in the environment: a review, Front. Environ. Sci. 10 (2023) 1058053, https://doi.org/10.3389/fenvs.2022.1058053.
[3] I.A. Bhatti, M.A. Hayat, M. Iqbal, Assessment of thorium in the environment (a review), J. Chem. Soc. Pak. 34 (2012) 1012–1022.
[4] Z. Zhu, Y. Pranolo, C.Y. Cheng, Separation of uranium and thorium from rare earths for rare earth production - A review, Miner. Eng. 77 (2015) 185–196, https://doi.org/10.1016/j.mineng.2015.03.012.
[5] A. Vengosh, R.M. Coyte, J. Podgorski, T.M. Johnson, A critical review on the occurrence and distribution of the uranium- and thorium-decay nuclides and their effect on the quality of groundwater, Sci. Total Environ. 808 (2022) 151914, https://doi.org/10.1016/j.scitotenv.2021.151914.
[6] "Ensuring Nuclear Performance", Molten Salt Reactor Research Program, https://www.ensuringnuclearperformance.com/en/nuclear-innovation/msr-research-program, Accessed: 01/15/2024.
[7] IAEA, Thorium fuel cycle - Potential benefits and challenges, in: IAEA (Ed.), International Atomic Energy Agency, Vienna (Austria), 2005, pp. 113.
[8] S. Mallapaty, China prepares to test thorium-fuelled nuclear reactor, Nature 597 (2021) 311–312, https://doi.org/10.1038/d41586-021-02459-w.
[9] E.H. Borai, M.S. Abd El-Ghany, I.M. Ahmed, M.M. Hamed, A.M.S. El-Din, H.F. Aly, Modified acidic leaching for selective separation of thorium, phosphate and rare earth concentrates from Egyptian crude monazite, Int. J. Miner. Process. 149 (2016) 34–41, https://doi.org/10.1016/j.minpro.2016.02.003.
[10] I. Kursun, M. Terzi, T.D. Tombal, HCl leaching behaviour of a bastnasite ore in terms of thorium and rare earth elements, Russ. J. Non-Ferrous Met. 57 (2016) 187–194, https://doi.org/10.3103/s106782121603010x.
[11] J. Demol, E. Ho, G. Senanayake, Sulfuric acid baking and leaching of rare earth elements, thorium and phosphate from a monazite concentrate: Effect of bake temperature from 200 to 800 °C, Hydrometall. 179 (2018) 254–267, https://doi.org/10.1016/j.hydromet.2018.06.002.
[12] Z. Liu, T. Xiu, Y. Du, Y. Wang, Leaching characteristics and kinetics of radioactive element uranium and thorium from Ta/Nb tailing, J. Radioanal. Nucl. Chem. 323 (2020) 1197–1206, https://doi.org/10.1007/s10967-020-07016-9.
[13] E. Kukkonen, E.J. Virtanen, J.O. Moilanen, α-Aminophosphonates, -phosphinates, and -phosphine oxides as extraction and precipitation agents for rare earth metals, thorium, and uranium: A review, Molecules 27 (2022) 3465, https://doi.org/10.3390/molecules27113465.
[14] N.T. Hung, L.B. Thuan, T.C. Thanh, M. Watanabe, D.V. Khoai, N.T. Thuy, H. Nhuan, P.Q. Minh, T.H. Mai, N.V. Tung, et al., Separation of thorium and uranium from xenotime leach solutions by solvent extraction using primary and tertiary amines, Hydrometall. 198 (2020) 105506, https://doi.org/10.1016/j.hydromet.2020.105506.
[15] K.W. Chung, H.-S. Yoon, C.-J. Kim, J.-Y. Lee, R.K. Jyothi, Solvent extraction, separation and recovery of thorium from Korean monazite leach liquors for nuclear industry applications, J. Ind. Eng. Chem. 83 (2020) 72–80, https://doi.org/10.1016/j.jiec.2019.11.014.
[16] S. Zafar, N. Khalid, M.L. Mirza, Sequestering of thorium ions from aqueous media on rice husk: Equilibrium, kinetic and thermodynamic studies, Radiochim. Acta 103 (2015) 385–395, https://doi.org/10.1515/ract-2014-2294.
[17] B.R. Broujeni, A. Nilchi, A.H. Hassani, R. Saberi, Preparation and characterization of chitosan/Fe_2O_3 nano composite for the adsorption of thorium (IV) ion from aqueous solution, Water Sci. Technol. 78 (2018) 708–720, https://doi.org/10.2166/wst.2018.343.

[18] G. Salunkhe, R.S. Chauhan, A. Sengupta, The application of food/agro-waste and spent household products for the environmentally benign separation of thorium, Environ. Sci.: Adv. 1 (2022) 546–557, https://doi.org/10.1039/d2va00067a.

[19] D. Hritcu, D. Humelnicu, G. Dodi, M.I. Popa, Magnetic chitosan composite particles: Evaluation of thorium and uranyl ion adsorption from aqueous solutions, Carbohydr. Polym. 87 (2012) 1185–1191, https://doi.org/10.1016/j.carbpol.2011.08.095.

[20] D. Humelnicu, C. Blegescu, D. Ganju, Removal of uranium(VI) and thorium(IV) ions from aqueous solutions by functionalized silica: kinetic and thermodynamic studies, J. Radioanal. Nucl. Chem. 299 (2014) 1183–1190, https://doi.org/10.1007/s10967-013-2873-4.

[21] D.L. Guerra, R.R. Viana, C. Airoldi, Use of raw and chemically modified hectorites as adsorbents for Th(IV), U(VI) and Eu(III) uptake from aqueous solutions, Desalination 260 (2010) 161–171, https://doi.org/10.1016/j.desal.2010.04.045.

[22] Z. Yang, G. Chen, H. Weng, W. Shen, Z. Huang, M. Lin, Efficient and selective separation of U(VI) and Th(IV) from rare earths using functionalized hierarchically mesoporous silica, J. Mater. Sci. - Mater. Electron. 53 (2018) 3398–3416, https://doi.org/10.1007/s10853-017-1808-9.

[23] S. Alharthi, Sequestering of radioactive thorium from wastewater using highly porous silica monoliths, JOM 74 (2022) 1035–1043, https://doi.org/10.1007/s11837-021-05100-3.

[24] T.S. Anirudhan, S. Rijith, A.R. Tharun, Adsorptive removal of thorium(IV) from aqueous solutions using poly(methacrylic acid)-grafted chitosan/bentonite composite matrix: Process design and equilibrium studies, Colloids Surf, A 368 (2010) 13–22, https://doi.org/10.1016/j.colsurfa.2010.07.005.

[25] M.O. Abd El-Magied, E.A. Elshehy, E.-S.-A. Manaa, A.A. Tolba, A.A. Atia, Kinetics and thermodynamics studies on the recovery of thorium ions using amino resins with magnetic properties, Ind. Eng. Chem. Res. 55 (2016) 11338–11345, https://doi.org/10.1021/acs.iecr.6b02977.

[26] G. Huang, Z. Chen, L. Wang, T. Lv, J. Shi, Removal of thorium(IV) from aqueous solution using magnetic ion-imprinted chitosan resin, J. Radioanal. Nucl. Chem. 310 (2016) 1265–1272, https://doi.org/10.1007/s10967-016-4993-0.

[27] K.L. Ang, D. Li, A.N. Nikoloski, The effectiveness of ion exchange resins in separating uranium and thorium from rare earth elements in acidic aqueous sulfate media. Part 1. Anionic and cationic resins, Hydrometall. 174 (2017) 147–155, https://doi.org/10.1016/j.hydromet.2017.10.011.

[28] A.L. Smirnov, S.M. Titova, V.N. Rychkov, G.M. Bunkov, V.S. Semenishchev, E. V. Kirillov, N.N. Poponin, I.A. Svirsky, Study of scandium and thorium sorption from uranium leach liquors, J. Radioanal. Nucl. Chem. 312 (2017) 277–283, https://doi.org/10.1007/s10967-017-5234-x.

[29] K.L. Ang, D. Li, A.N. Nikoloski, The effectiveness of ion exchange resins in separating uranium and thorium from rare earth elements in acidic aqueous sulfate media. Part 2. Chelating resins, Miner. Eng. 123 (2018) 8–15, https://doi.org/10.1016/j.mineng.2018.04.017.

[30] K. Arora, S. Agnihotri, Thorium(IV) metal complexes with neutral nitrogen donor ligands - A review, Asian J. Chem. 19 (2007) 3307–3324.

[31] R.K. Agarwal, H. Agarwal, K. Arora, Thorium (IV) metal complexes with neutral oxygen donor ligands - A review, Rev. Inorg. Chem. 20 (2000) 1–61, https://doi.org/10.1515/REVIC.2000.20.1.1.

[32] C.D. Tutson, A.E.V. Gorden, Thorium coordination: A comprehensive review based on coordination number, Coord. Chem. Rev. 333 (2017) 27–43, https://doi.org/10.1016/j.ccr.2016.11.006.

[33] S.I. El-Dessouky, E.H. Borai, Extraction chromatography of thorium ion by solid phase impregnated resins containing bi-functional organic extractants, J. Radioanal. Nucl. Chem. 268 (2006) 247–254, https://doi.org/10.1556/jrnc.268.2006.2.11.

[34] Y. Wang, X. Chen, X. Hu, P. Wu, T. Lan, Y. Li, H. Tu, Y. Liu, D. Yuan, Z. Wu, et al., Synthesis and characterization of poly(TRIM/VPA) functionalized graphene oxide nanoribbons aerogel for highly efficient capture of thorium(IV) from aqueous solutions, Appl. Surf. Sci 536 (2021) 147829, https://doi.org/10.1016/j.apsusc.2020.147829.

[35] A.M. Atta, Z.F. Akl, Removal of thorium from water using modified magnetite nanoparticles capped with rosin amidoxime, Mater. Chem. Phys. 163 (2015) 253–261, https://doi.org/10.1016/j.matchemphys.2015.07.038.

[36] B.R. Broujeni, A. Nilchi, Preparation and characterization of polyacrylonitrile/aluminum oxide nanofiber adsorbent modified with 2-amino-3-methyl-1-hexanethiol for the adsorption of thorium (IV) ion from aqueous solution, J. Environ. Eng. 144 (2018) 04018099, https://doi.org/10.1061/(asce)ee.1943-7870.0001446.

[37] R.G. Pearson, Acids and bases, Science (New York, N.Y.), 151 (1966) 172-177. https://doi.org/10.1126/science.151.3707.172.

[38] A. Baimenov, D.A. Berillo, S.G. Poulopoulos, V.J. Inglezakis, A review of cryogels synthesis, characterization and applications on the removal of heavy metals from aqueous solutions, Adv. Colloid Interface Sci. 276 (2020) 102088, https://doi.org/10.1016/j.cis.2019.102088.

[39] M.-A. Gatou, P. Bika, T. Stergiopoulos, P. Dallas, E.A. Pavlatou, Recent advances in covalent organic frameworks for heavy metal removal applications, Energies 14 (2021) 3197, https://doi.org/10.3390/en14113197.

[40] S. Jakavula, N.R. Biata, M. Dimp, V.E. Pakade, P.N. Nomngongo, A critical review on the synthesis and application of ion-imprinted polymers for selective preconcentration, speciation, removal and determination of trace and essential metals from different matrices, Crit. Rev. Anal. Chem. 52 (2022) 314–326, https://doi.org/10.1080/10408347.2020.1798210.

[41] M.S. Khan, S.E.Z. Syeda, A.M. Skwierawska, Recent advancements in molecularly imprinted polymers for the removal of heavy metal ions and dyes, Desalin. Water Treat. 289 (2023) 123–144, https://doi.org/10.5004/dwt.2023.29458.

[42] S. Selambakkannu, N.A.F. Othman, T.M. Ting, N.H. Mohamed, A. Hashim, Z. A. Karim, Preparation and optimization of thorium selective ion imprinted nonwoven fabric grafted with poly(2-dimethylaminoethyl methacrylate) by electron beam irradiation technique, J. Environ. Chem. Eng. 8 (2020) 103737, https://doi.org/10.1016/j.jece.2020.103737.

[43] N.A.F. Othman, S. Selambakkannu, H. Azian, C.T. Ratnam, T. Yamanobe, H. Hoshina, N. Seko, Synthesis of surface ion-imprinted polymer for specific detection of thorium under acidic conditions, Polym. Bull. 78 (2021) 165–183, https://doi.org/10.1007/s00289-019-03094-2.

[44] B. Bingöl, W.H. Meyer, M. Wagner, G. Wegner, Synthesis, microstructure, and acidity of poly(vinylphosphonic acid), Macromol. Rapid Commun. 27 (2006) 1719–1724, https://doi.org/10.1002/marc.200600513.

[45] A. Saeed, D.M.R. Georget, A.G. Mayes, Synthesis, characterisation and solution thermal behaviour of a family of poly (N-isopropyl acrylamide-co-N-hydroxymethyl acrylamide) copolymers, React. Funct. Polym. 70 (2010) 230–237, https://doi.org/10.1016/j.reactfunctpolym.2009.12.004.

[46] H. Erdemi, A. Bozkurt, Synthesis and characterization of poly(vinylpyrrolidone-co-vinylphosphonic acid) copolymers, Eur. Polym. J. 40 (2004) 1925–1929, https://doi.org/10.1016/j.eurpolymj.2004.04.001.

[47] M. Farrokhi, M. Abdollahi, Enhancing medium/high temperature proton conductivity of poly(benzimidazole)-based proton exchange membrane via blending with poly(vinyl imidazole-co-vinyl phosphonic acid) copolymer: Proton conductivity-copolymer microstructure relationship, Eur. Polym. J. 131 (2020) 109691, https://doi.org/10.1016/j.eurpolymj.2020.109691.

[48] T.S. Anirudhan, S.S. Sreekumari, S. Jalajamony, An investigation into the adsorption of thorium(IV) from aqueous solutions by a carboxylate-functionalised graft copolymer derived from titanium dioxide-densified cellulose, J. Environ. Radioact. 116 (2013) 141–147, https://doi.org/10.1016/j.jenvrad.2012.10.001.

[49] E. Birlik, S. Buyuktiryaki, A. Ersoz, A. Denizli, R. Say, Selective separation of thorium using ion imprinted chitosan-phthalate particles via solid phase extraction, Sep. Sci. Technol. 41 (2006) 3109–3121, https://doi.org/10.1080/01496390600851400.

[50] T.P. Rao, R. Kala, S. Daniel, Metal ion-imprinted polymers—Novel materials for selective recognition of inorganics, Anal. Chim. Acta 578 (2006) 105–116, https://doi.org/10.1016/j.aca.2006.06.065.

[51] M.M. Lazar, C.-A. Ghiorghita, E.S. Dragan, D. Humelnicu, M.V. Dinu, Ion-imprinted polymeric materials for selective adsorption of heavy metal ions from aqueous solution, Molecules 28 (2023) 2798.

[52] E.J. Virtanen, S. Peramaki, K. Helttunen, A. Vaisanen, J.O. Moilanen, Alkyl-substituted aminobis(phosphonates)-efficient precipitating agents for rare earth elements, thorium, and uranium in aqueous solutions, ACS Omega 6 (2021) 23977–23987, https://doi.org/10.1021/acsomega.1c02982.

[53] Y. Chen, Y. Chen, D. Lu, Y. Qiu, Synthesis of a novel water-soluble polymer complexant phosphorylated chitosan for rare earth complexation, Polymers 14 (2022) 419, https://doi.org/10.3390/polym14030419.

[54] L.-P. Xiong, M. Gu, C.-T. Yang, K. Lv, F.-C. Wu, S. Hu, X.-G. Long, Metal phosphonate sorbents: Enhancement of actinide sorption performance by gamma irradiation, Chem. Eng. J. 430 (2022) 132753, https://doi.org/10.1016/j.cej.2021.132753.

[55] G. Zante, V. Bouniol, S. Sene, C. Rey, J. Causse, J. Larionova, Y. Guari, X. Deschanels, S. Le Caër, Grafted mesoporous silicas for radionuclide uptake: Radiolytic stability under electron irradiation, Microporous Mesoporous Mater. 336 (2022) 111851, https://doi.org/10.1016/j.micromeso.2022.111851.

[56] S. Sun, D. Zou, J. Chen, Y. Deng, Study of removing radioactive thorium(IV) from high-purity scandium(III) products with di-(2-ethylhexyl) 2-ethylhexyl phosphonate (DEHEHP) in nitric acid solution, Hydrometall. 222 (2023), https://doi.org/10.1016/j.hydromet.2023.106176.

[57] X. Yang, S. Wang, L. Xu, C. Liu, C. Jin, A. Zhang, C. Xiao, Extraction and complexation mechanism of uranium(VI) and thorium(IV) by tetradentate phenanthroline phosphonate (POPhen) ligands, Sep. Purif. Technol. 320 (2023), https://doi.org/10.1016/j.seppur.2023.124124.

[58] J.H. Maas, M.A. Cohen Stuart, A.B. Sieval, H. Zuilhof, E.J.R. Sudhölter, Preparation of polystyrene brushes by reaction of terminal vinyl groups on silicon and silica surfaces, Thin Solid Films 426 (2003) 135–139, https://doi.org/10.1016/S0040-6090(03)00033-6.

[59] M. Thommes, K. Kaneko, A.V. Neimark, J.P. Olivier, F. Rodriguez-Reinoso, J. Rouquerol, K.S.W. Sing, Physisorption of gases, with special reference to the evaluation of surface area and pore size distribution (IUPAC Technical Report), Pure Appl. Chem. 87 (2015) 1051–1069, https://doi.org/10.1515/pac-2014-1117.

[60] H. Liang, Q. Chen, J. Ma, Y. Huang, X. Shen, Synthesis and characterization of a new ion-imprinted polymer for the selective separation of thorium(IV) ions at high acidity, RSC Adv. 7 (2017) 35394–35402, https://doi.org/10.1039/c7ra05061e.

[61] N.B. Colthup, L.H. Daly, S.E. Wiberley, Introduction to Infrared and Raman Spectroscopy, 3rd. ed., Academic Press Inc, San Diego, CA (USA), 1990, p. 560.

[62] R. Quiñones, S. Garretson, G. Behnke, J.W. Fagan, K.T. Mueller, S. Agarwal, R. K. Gupta, Fabrication of phosphonic acid films on nitinol nanoparticles by dynamic covalent assembly, Thin Solid Films 642 (2017) 195–206, https://doi.org/10.1016/j.tsf.2017.09.048.

[63] M. Monier, D.A. Abdel-Latif, Synthesis and characterization of ion-imprinted resin based on carboxymethyl cellulose for selective removal of UO_2^{2+}, Carbohydr. Polym. 97 (2013) 743–752, https://doi.org/10.1016/j.carbpol.2013.05.062.

[64] D.S. Wishart, A. Guo, E. Oler, F. Wang, A. Anjum, H. Peters, R. Dizon, Z. Sayeeda, S. Tian, B.L. Lee, et al., HMDB 5.0: the human metabolome database for 2022, Nucleic Acids Res 50 (2022) D622–D631, https://doi.org/10.1093/nar/gkab1062.

[65] C. Moulin, B. Amekraz, S. Hubert, V. Moulin, Study of thorium hydrolysis species by electrospray-ionization mass spectrometry, Anal. Chim. Acta 441 (2001) 269–279, https://doi.org/10.1016/S0003-2670(01)01084-4.
[66] H. Moon, Equilibrium ultrafiltration of hydrolyzed thorium(IV) solutions, Bull. Korean Chem. Soc. 10 (1989) 270–272.
[67] C.F. Baes, Jr., R.E. Mesmer, Hydrolysis of Cations, Wiley, NY, 1976, pp.
[68] T. Sasaki, Y. Takaoka, T. Kobayashi, T. Fujii, I. Takagi, H. Moriyama, Hydrolysis constants and complexation of Th(IV) with carboxylates, Radiochim. Acta 96 (2008) 799–803, https://doi.org/10.1524/ract.2008.1523.
[69] H. Nisbet, A. Migdisov, H. Xu, X. Guo, V. van Hinsberg, A.E. Williams-Jones, H. Boukhalfa, R. Roback, An experimental study of the solubility and speciation of thorium in chloride-bearing aqueous solutions at temperatures up to 250 °C, Geochim. Cosmochim. Acta 239 (2018) 363–373, https://doi.org/10.1016/j.gca.2018.08.001.
[70] S. Azizian, Kinetic models of sorption: a theoretical analysis, J. Colloid Interface Sci. 276 (2004) 47–52, https://doi.org/10.1016/j.jcis.2004.03.048.
[71] G. Blanchard, M. Maunaye, G. Martin, Removal of heavy metals from waters by means of natural zeolites, Water Res. 18 (1984) 1501–1507, https://doi.org/10.1016/0043-1354(84)90124-6.
[72] J. Wang, X. Guo, Adsorption kinetic models: Physical meanings, applications, and solving methods, J. Hazard. Mater. 390 (2020) 122156, https://doi.org/10.1016/j.jhazmat.2020.122156.
[73] S. Salvestrini, A modification of the Langmuir rate equation for diffusion-controlled adsorption kinetics, React. Kinet. Mech. Catal. 128 (2019) 571–586, https://doi.org/10.1007/s11144-019-01684-9.
[74] H.N. Tran, S.J. You, A. Hosseini-Bandegharaei, H.P. Chao, Mistakes and inconsistencies regarding adsorption of contaminants from aqueous solutions: A critical review, Water Res. 120 (2017) 88–116, https://doi.org/10.1016/j.watres.2017.04.014.
[75] M.A. Hubbe, S. Azizian, S. Douven, Implications of apparent pseudo-second-order adsorption kinetics onto cellulosic materials: A review, BioResources 14 (2019) 7582–7627, https://doi.org/10.15376/biores.14.3.7582-7626.
[76] H.Y. Sharef, A.F. Jalal, B.M. Ibrahim, N.A. Fakhre, I.N. Qader, New ion-imprinted polymer for selective removal of Cu^{2+} ion in aqueous solution using extracted *Aloe vera* leaves as a monomer, Int. J. Biol. Macromol. 239 (2023) 124318, https://doi.org/10.1016/j.ijbiomac.2023.124318.
[77] N.Z. Misak, Some aspects of the application of adsorption isotherms to ion exchange reactions, React. Funct. Polym. 43 (2000) 153–164, https://doi.org/10.1016/S1381-5148(99)00046-2.
[78] S. Salvestrini, L. Ambrosone, F.D. Kopinke, Some mistakes and misinterpretations in the analysis of thermodynamic adsorption data, J. Mol. Liq. 352 (2022) 118762, https://doi.org/10.1016/j.molliq.2022.118762.
[79] H.N. Tran, E.C. Lima, R.-S. Juang, J.-C. Bollinger, H.-P. Chao, Thermodynamic parameters of liquid-phase adsorption process calculated from different equilibrium constants related to adsorption isotherms: A comparison study, J. Environ. Chem. Eng. 9 (2021) 106674, https://doi.org/10.1016/j.jece.2021.106674.
[80] N.H. Elsayed, M. Monier, R.A.S. Alatawi, M. Al-Anazi, M. Albalawi, M.J. Alatawi, Selective removal of uranyl ions using ion-imprinted amino-phenolic functionalized chitosan, Int. J. Biol. Macromol. 237 (2023) 124073, https://doi.org/10.1016/j.ijbiomac.2023.124073.
[81] B.R. Broujeni, A. Nilchi, A.H. Hassani, R. Saberi, Application of chitosan/Al_2O_3 nano composite for the adsorption of thorium (IV) ion from aqueous solution, Desalin. Water Treat. 106 (2018) 125–133, https://doi.org/10.5004/dwt.2018.21760.
[82] C. Siva Kesava Raju, M.S. Subramanian, Sequential separation of lanthanides, thorium and uranium using novel solid phase extraction method from high acidic nuclear wastes, J. Hazard. Mater. 145 (2007) 315–322, https://doi.org/10.1016/j.jhazmat.2006.11.024.
[83] D. Yuan, S. Zhang, Z. Xiang, Y. He, Y. Wang, Y. Liu, X. Zhao, X. Zhou, Q. Zhang, Highly efficient removal of thorium in strong HNO_3 media using a novel polymer adsorbent bearing a phosphonic acid ligand: a combined experimental and density functional theory study, ACS Appl. Mater. Interfaces 11 (2019) 24512–24522, https://doi.org/10.1021/acsami.9b03674.
[84] M. Sharma, P. Sharma, L. Yadav, V.C. Janu, R. Gupta, Sequestration and recovery of thorium ions using a recyclable, low-cost, glutathione-based magnetic nanocomposite: Experimental study and statistical modeling, Sep. Purif. Technol. 322 (2023) 124264, https://doi.org/10.1016/j.seppur.2023.124264.
[85] M.F. Hamza, E. Guibal, Y. Wei, S. Ning, Synthesis, characterization, and evaluation of thiocarbazide-functionalized maleic-based polymer for thorium (IV) removal from aqueous solutions, Chem. Eng. J. 464 (2023) 142638, https://doi.org/10.1016/j.cej.2023.142638.
[86] E. Nieboer, D.H.S. Richardson, The replacement of the non-descript therm heavy-metals by a biologically and chemically significant classification of metal-ions, Environ. Pollut. Series B 1 (1980) 3–26, https://doi.org/10.1016/0143-148x(80)90017-8.
[87] K. Li, M. Li, D. Xue, Solution-phase electronegativity scale: Insight into the chemical behaviors of metal ions in solution, J. Phys. Chem. A 116 (2012) 4192–4198, https://doi.org/10.1021/jp300603f.
[88] F.F. He, H.Q. Wang, Y.Y. Wang, X.F. Wang, H.S. Zhang, H.L. Li, J.H. Tang, Magnetic Th(IV)-ion imprinted polymers with salophen schiff base for separation and recognition of Th(IV), J. Radioanal. Nucl. Chem. 295 (2013) 167–177, https://doi.org/10.1007/s10967-012-1891-y.
[89] C. Lin, H. Wang, Y. Wang, Z. Cheng, Selective solid-phase extraction of trace thorium(IV) using surface-grafted Th(IV)-imprinted polymers with pyrazole derivative, Talanta 81 (2010) 30–36, https://doi.org/10.1016/j.talanta.2009.11.032.
[90] E.M. Verdugo, Y. Xie, J. Baltrusaitis, D.M. Cwiertny, Hematite decorated multi-walled carbon nanotubes (α-Fe_2O_3/MWCNTs) as sorbents for Cu(II) and Cr(VI): comparison of hybrid sorbent performance to its nanomaterial building blocks, RSC Adv. 6 (2016) 99997–100007, https://doi.org/10.1039/c6ra16332g.
[91] V. Devi, M. Selvaraj, P. Selvam, A.A. Kumar, S. Sankar, K. Dinakaran, Preparation and characterization of CNSR functionalized Fe_3O_4 magnetic nanoparticles: An efficient adsorbent for the removal of cadmium ion from water, J. Environ. Chem. Eng. 5 (2017) 4539–4546, https://doi.org/10.1016/j.jece.2017.08.036.
[92] X.Y. Jiang, H.Q. Wang, Q.L. Wang, E.M. Hu, Y.Q. Duan, Immobilizing amino-functionalized mesoporous silica into sodium alginate for efficiently removing low concentrations of uranium, J. Cleaner Prod. 247 (2020) 119162, https://doi.org/10.1016/j.jclepro.2019.119162.
[93] J.C. Steinbach, F. Fait, H.A. Mayer, A. Kandelbauer, Monodisperse porous silica/polymer nanocomposite microspheres with tunable silica loading, morphology and porosity, Int. J. Mol. Sci. 23 (2022) 14977, https://doi.org/10.3390/ijms232314977.
[94] J. Bai, Y. Huang, Q. Gong, X. Liu, Y. Li, J. Gan, M. Zhao, Y. Shao, D. Zhuang, J. Liang, Preparation of porous carbon nanotube/carbon composite spheres and their adsorption properties, Carbon 137 (2018) 493–501, https://doi.org/10.1016/j.carbon.2018.05.058.
[95] W. Cao, H. Li, Y. Hong, Z. Yang, M. Fu, Preparation and characterization of spherical lignocellulose-based anion exchanger from sugarcane bagasse, BioResources 17 (2022) 3984–4000, https://doi.org/10.15376/biores.17.3.3984-4000.
[96] T. Bugdayci, S. Bektas, E.T. Akgul, B. Korkmaz, E. Yavuz, B.F. Senkal, Urethane- and urea-modified polymeric sorbents enable efficient and selective removal of mercury(II) from water, Polym. Bull. 80 (2023) 12079–12102, https://doi.org/10.1007/s00289-022-04642-z.
[97] D. Schwarz, J. Weber, Synthesis of mesoporous poly(melamine-formaldehyde) particles by inverse emulsion polymerization, J. Colloid Interface Sci. 498 (2017) 335–342, https://doi.org/10.1016/j.jcis.2017.03.064.